This is an author produced version of a paper published in **Physics of Fluids.**

Ignition of thermally-sensitive explosives between a contact surface and a shock.

Gary J. Sharpe†& Mark Short‡

†*School of Mechanical Engineering,*

University of Leeds,

Leeds, LS2 9JT, UK.

Email: mengjs@leeds.ac.uk.

‡*Los Alamos National Laboratory,*

Los Alamos, New Mexico,

NM 87545, USA.

(Dated: March 15, 2008)

Abstract

The dynamics of ignition between a contact surface and a shock wave is investigated using a one-step reaction model with Arrhenius kinetics. Both large activation energy asymptotics and high-resolution finite activation energy numerical simulations are employed. Emphasis is on comparing and contrasting the solutions with those of the ignition process between a piston and a shock, considered previously. The large activation energy asymptotic solutions are found to be qualitatively different from the piston driven shock case, in that thermal runaway first occurs ahead of the contact surface, and both forward and backward moving reaction waves emerge. These waves take the form of quasi-steady weak detonations that may later transition into strong detonation waves. For the finite activation energies considered in the numerical simulations, the results are qualitatively different to the asymptotic predictions in that no backward weak detonation wave forms, and there is only a weak dependence of the evolutionary events on the acoustic impedance of the contact surface. The above conclusions are relevant to gas phase equation of state models. However, when a large polytropic index more representative of condensed phase explosives is used, the large activation energy asymptotic and finite activation energy numerical results are found to be in quantitative agreement.

I. INTRODUCTION

Ignition of explosive fuels by the passage of a shock wave is an important issue from the perspective of safety (e.g. storage and handling). For fuels which can be characterized by a single exothermic reaction model with an Arrhenius form of the reaction rate, the evolutionary mechanisms of the shock-to-detonation transition process are well understood in the case that the shock is driven by a constant velocity piston, or equivalently by the reflection of a weaker shock from a stationary wall.

Indeed, a complete theoretical picture of the shock-to-detonation transition process exists for the asymptotic limit of large activation energy of the reaction [1–3]. This theory shows that the evolution begins with an induction stage during which the shocked material slowly evolves from the uniform initial shocked state due to weak heat release. This stage ends with a thermal runaway event at the piston (where the material has been shocked for the longest). The fuel subsequently burns to complete reaction on a timescale which is exponentially short compared to the induction time. However, this thermal runaway event is just the first in a series of local thermal runaways, which occur sequentially due to a gradient in induction times created by the passage of the shock. A locus of thermal runaways thus moves away from the initial point of runaway, which represents the leading order the path of a weak detonation wave (a shockless reaction wave which is supersonic throughout in its own rest frame) [1–3]. Since the reaction rates are exponentially rapid in the high activation energy limit, this wave is assumed quasi-steady, i.e. the particle transit time through the wave is short compared to the evolution time of the wave. This quasi-steady weak detonation decelerates very rapidly, and once it reaches the Chapman-Jouguet (CJ) speed, a sonic point appears in the region of reaction burnout [1]. At this point unsteady effects become important, which results in the formation of a secondary shock. This interior shock subsequently accelerates, and propagates rapidly through the remaining part of the upstream weak detonation, transforming it into a strong detonation [1]. This theory predicts that the strong detonation forms very close to the piston in gaseous fuels [2].

However, numerical simulations of the piston driven shock-to-detonation process with finite, but realistic activation energies [4, 5] show qualitatively different evolution scenarios than that predicted by the asymptotic theory . For moderately large activation energies, the reaction wave which emerges from the piston face consists only partially of a quasi-steady

2

weak detonation, with the remainder of the wave complex comprising an unsteady combustion zone followed by part of a quasi-steady fast-flame (an expansive, subsonic reaction wave). Due to this unsteadiness, the secondary shock forms internal to the reaction wave complex, sometimes closer to the head of the wave complex than to the rear, and the spatial location of the shock formation may be orders of magnitude further from the piston face than the asymptotic prediction. As the effective activation energy is decreased (e.g. as the strength of the initiating shock increases), the region of the reaction wave consisting of a weak detonation rapidly diminishes, and the wave becomes more and more unsteady. The points of formation of the secondary shock and strong detonation also move further from the piston face and closer to the initiating shock [5].

The disparity between the large activation energy asymptotic picture and the finite activation energy calculations is due to the assumption in the asymptotics that the reaction wave which emerges from the induction phase is quasi-steady. In the high activation energy limit, the weak detonation decelerates extremely rapidly, and hence the secondary shock forms extremely close to the piston face [2]. For such rapid decelerations, the post-shock temperature scaled activation energy would need to be very high in order for the main reaction zone to be sufficiently thin that the quasi-steady approximation holds. For the finite activation energies considered in [4, 5], the main reaction zone times are not short compared to the asymptotic wave deceleration time, and hence unsteadiness needs to be considered, which profoundly affects the evolution [5].

A more general problem than the piston driven shock case described above is that of ignition between a contact surface and a shock. This scenario arises, for example, when two weak shocks merge, producing an expansion wave, contact surface, and stronger shock triad [6, 7] with an increased temperature (and hence shorter induction time) in the region between the contact surface and the shock. This occurs, for example, in the deflagration-to-detonation transition experiments of Urtiew & Oppenheim [8], where an accelerating flame produces a series of shocks which subsequently merge. It also can occur as part of the piston driven shock initiation scenario itself, when the secondary shock formed in the ignition process overtakes the original initiating shock [5]. In addition, the contact-shock problem arises in shock-initiation experiments on condensed phase (solid and liquid) explosives. In these experiments, a gas gun is used to drive flier plates into the explosive, e.g. [10, 11]. Upon contact, the impact produces a shock in the explosive and a shock wave travelling

3

back into the projectile; the contact surface is the material interface between projectile and explosive. Another scenario where the contact-shock configuration occurs is in shock tubes when a diaphragm between a higher pressure driver gas and the explosive gas is burst, again producing an expansion, contact and shock triad, e.g. [12]. A related problem occurs in the failure and subsequent re-ignition of a strong detonation wave [13]. In the failing strong detonation, the shock and reaction decouple into a weak shock and a fast-flame, with the latter acting as a contact discontinuity separating the induction zone behind the weak shock from the burnt products. The strong regime of shock-induced ignition in gaseous explosives and the flier plate experiments in condensed phase explosives are reproducible, essentially one-dimensional events [8, 11].

In ignition between a contact surface and shock, the role of the contact surface is to enhance chemical reaction by partially reflecting acoustic pressure waves created by the evolution of the induction zone ahead of it. These waves are also partially transmitted into the material behind the contact surface. Thus the contact-shock problem is more general than the problem of ignition between a piston and a shock. The former includes an extra variable, namely the acoustic impedance of the material behind the contact surface[6]. In fact, the more general contact-shock problem includes the piston driven shock case considered previously. The latter is recovered in the limit of infinite acoustic impedance behind the contact surface [6].

Solutions of the contact-shock problem have been obtained in the large activation energy asymptotic limit [2, 6, 7, 9], which are described more fully in §III below. The induction time is found to increase as the acoustic impedance of the contact surface decreases, due to larger acoustic leakage through the contact surface. However, in contrast to the piston driven shock case, the point of first thermal runaway may occur not at the contact surface itself, but a small distance ahead of it. Thus, somewhat counter-intuitively, the particle which has been shocked the longest is not necessarily the first one to reach ignition. The reason is that, as the temperature begins to rise, the material is able to expand locally near the contact surface more readily than in the piston case due to the finite impedance of the contact surface. This results in a relative deceleration of the contact surface, and a competition develops between expansion of the material and heat accumulation, thus delaying ignition at the contact surface [6]. However, the first ignition still occurs close to the contact surface, and, furthermore, the maximum in temperature remains at the contact surface until close

4

to the thermal runaway time. As the acoustic impedance of the contact surface is increased, the point of first runaway moves closer to it [6, 7, 9].

In the asymptotic solution of the contact-shock ignition problem, particles subsequently runaway sequentially in both the upstream and downstream directions from this first point of ignition. This signifies weak detonations moving both forward and backward away from this point. The forward moving wave still decelerates rapidly, but not as quickly as in the piston driven shock scenario. However, the backward weak detonation that moves towards the contact surface is found to decelerate much more rapidly than the forward moving wave, so that, despite the very small distance between the contact surface and the origin of the wave, its speed still drops significantly before it reaches the contact surface. Depending on the acoustic impedance, the weak detonation may slow to the CJ speed before it reaches the contact surface. In such cases this would signify the birth of a strong detonation wave moving towards the contact surface.

Due to the very small length and time scales involved in the asymptotic solutions, i.e. the very small distance between the contact surface and the point of first runaway, and the rapidity of the deceleration of the backward weak detonation, very high post-shock temperature scaled activation energies would be required for the main reaction stage to be thin compared to these scales, and hence for the assumptions of the asymptotics to be realized. Furthermore, given the qualitative differences between the large activation energy asymptotic and finite activation energy numerical solutions that appear even in the piston case (where the backward wave, and its associated smaller scales, do not appear), one would also expect that the numerical solutions for large, but finite activation energies would be profoundly different to those identified in the high activation energy limit for the ignition between a contact surface and shock wave.

Previous numerical simulations of the contact-shock initiation scenarios have been performed for various finite activation energy chemical kinetic models [12, 14]. These simulations indicate that ignition may indeed occur ahead of the contact surface, resulting in reaction waves moving in both directions. However, due to the temperature sensitive nature of the induction region, and to the very small scales which may be inherent in the solution (as indicated by asymptotic analysis for one-step Arrhenius chemistry), very high resolution simulations will be required to resolve the ignition dynamics on these fine scales. In this paper, high resolution, detailed numerical simulations are performed using a one-step

Arrhenius reaction model, such that the ignition dynamics near the contact surface are, for the first time, properly resolved. We examine how the evolution depends on the activation energy, and compare and contrast these finite activation energy numerical results with the large activation energy asymptotic predictions, as well as with the piston driven shock initiation numerical solutions. The plan of the paper is as follows: in §II the governing equations of the model are given; the asymptotic solutions are briefly described in §III; the results of the numerical simulations are examined in §IV; §V contains the conclusions.

II.   GOVERNING EQUATIONS

We consider the standard model system consisting of one irreversible reaction, A→B, with an Arrhenius form of the reaction rate. In one-dimension, the dimensionless versions of the governing equations are

$$\frac{\partial \rho}{\partial t} + u\frac{\partial \rho}{\partial x} + \rho\frac{\partial u}{\partial x} = 0, \tag{1}$$

$$\frac{\partial u}{\partial t} + u\frac{\partial u}{\partial x} + \frac{1}{\rho}\frac{\partial p}{\partial x} = 0, \tag{2}$$

$$\frac{\partial e}{\partial t} + u\frac{\partial e}{\partial x} - \frac{p}{\rho^2}\left[\frac{\partial \rho}{\partial t} + u\frac{\partial \rho}{\partial x}\right] = 0, \tag{3}$$

$$\frac{\partial \lambda}{\partial t} + u\frac{\partial \lambda}{\partial x} = \frac{1}{(\gamma-1)QE}(1-\lambda)\exp(E[1-1/T]), \tag{4}$$

where u is the fluid velocity, ρ the density (with $V = 1/\rho$ the specific volume), p the pressure, e the internal energy per unit mass, λ the mass fraction of the product (so that $\lambda = 0$ in the unburnt state and $\lambda = 1$ in the completely burnt state), E and Q the dimensionless activation energy and heat of reaction, respectively, γ is the (constant) ratio of specific heats in the case of gaseous explosives, and

$$T = \frac{p}{\rho}$$

defines the temperature. The distance, x, and material velocity, u, in Eqns. 1-4 are measured with respect to a frame of reference to be specified below. We assume a polytropic equation of state so that the internal energy is given by

$$e(\rho, p, \lambda) = \frac{p}{(\gamma-1)\rho} - Q\lambda, \tag{5}$$

6

Note that such an equation of state model using a polytropic index of $\gamma \approx 3$ is also often employed as a simple, qualitative model of condensed phase explosives [15]. Eqns. 1-5 are supplemented by the standard Rankine-Hugoniot jumps conditions across shock waves and contact discontinuities.

Here we consider the scenario of a shock with initial Mach number M_0 propagating into a reactive material whose initial state is denoted by a zero subscript, and moving away from a contact discontinuity, behind which the density is initially ρ_B. The initial conditions correspond to the time at which the shock and contact surface separate. At this time the contact-shock complex is located at $x^l = 0$, where an l superscript denotes the laboratory frame (e.g. $x^l = 0$ is the point at which the shocks collide in the shock merging problem, or is the position of the diaphragm in the shock tube scenario). The initial state between the shock and contact surface (and hence also the initial pressure and material velocity immediately behind the contact surface) just after they separate is denoted by an s subscript. If there was no heat release (i.e. the inert case), the solution would be self-similar corresponding to a shock of constant speed moving away from the contact discontinuity, with a uniform state in between and with the density immediately behind the contact surface remaining at ρ_B. The (constant) speed at which the contact surface subsequently moves in the inert case is given by the post-shock particle speed in the laboratory frame, u_s^l, since a contact moves with the fluid.

In the corresponding reactive version, just after the shock and contact surface separate at $t = 0_+$, the contact surface will still move away from $x^l = 0$ with speed u_s^l. However, the contact surface will subsequently decelerate due to the thermal expansion induced by the exothermic reaction ahead of it, which is switched on by the passage of the shock. At very early times on the ignition time scale the configuration will remain close to the self-similar solution of the inert problem since the total heat released is then very small. Here we work in the non-accelerating rest frame of the contact surface in the inert version of the problem, or equivalently in the instantaneous rest frame of the contact at $t = 0_+$ for the reactive version. Hence in Eqns. 1-4, $x = x^l - u_s^l t$ denotes distance from the contact surface in the non-reactive solution. Similarly, $u = u^l - u_s^l$ measures the fluid speed relative to the contact surface's speed in the non-reaction solution. Thus for the inert version, the contact surface would remain stationary at $x = 0$, while in the reactive case it will be pushed backwards in this frame of reference by the thermal expansion of the reacting material ahead of it. Note

that, for infinite acoustic impedance of the contact surface, this is just the piston rest frame used in [5].

In contrast to the inert version, in the reactive ignition between a contact surface and a shock wave, the density just behind the contact surface will not remain at ρ_B, due to the partial transmission through it of acoustic waves induced by the heat release in the induction zone ahead of it.

Equations 1-5 have been non-dimensionalized using the following self-consistent scalings

$$\rho = \frac{\tilde{\rho}}{\tilde{\rho}_s}, \quad p = \frac{\tilde{p}}{\tilde{p}_s}, \quad T = \frac{p}{\rho} = \frac{\tilde{R}\tilde{\rho}_s}{\tilde{p}_s}\tilde{T}_s, \quad u = \left(\frac{\tilde{\rho}_s}{\tilde{p}_s}\right)^{1/2}\tilde{u},$$

where a tilde denotes dimensional quantities. The dimensionless upstream, quiescent state ahead of the shock (denoted by a zero subscript) is then given by the shock jump conditions as

$$\rho_0 = \frac{\gamma-1}{\gamma+1} + \frac{2}{(\gamma+1)M_0^2}, \quad p_0 = \frac{\gamma+1}{\gamma+1+2\gamma(M_0^2-1)}, \quad T_0 = p_0/\rho_0,$$

$$u_0 = (\rho_0-1)M_0\left(\frac{\gamma p_0}{\rho_0}\right)^{1/2}, \quad \lambda_0 = 0. \tag{6}$$

Time is non-dimensionalized using the high activation energy, spatially homogeneous constant volume explosion time corresponding to the initial shocked state[16], i.e.

$$t = \frac{\tilde{t}}{\tilde{t}_{\exp}}, \quad \tilde{t}_{\exp} = \frac{\tilde{C}_V \tilde{T}_s^2}{\tilde{k}\tilde{E}\tilde{Q}} \exp\left(\frac{\tilde{E}}{\tilde{T}_s}\right),$$

where $\tilde{k}$ is the dimensional rate multiplier and $\tilde{C}_V$ is the specific heat at constant volume.

Distance is then scaled as

$$x = \left(\frac{\tilde{\rho}_s}{\tilde{p}_s}\right)^{1/2}\frac{\tilde{x}}{\tilde{t}_{\exp}},$$

characteristic of the distance an acoustic wave disturbance would travel in the shocked material during time $t = 1$ ($\tilde{t} = \tilde{t}_{\exp}$). The dimensionless initial value of the density just behind the contact surface is then $\rho_B = \tilde{\rho}_B/\tilde{\rho}_s$, and the initial acoustic impedance, as defined in [6], of the material here is $\alpha_0 = \sqrt{\rho_B}$. The limit $\alpha_0 \to \infty$ corresponds to the constant velocity piston case considered previously.

In this paper, when unspecified, the parameter set considered is $\gamma = 1.4$, $Q = 4$, $M_0 = 1.5$, since these are the values considered in detail in both the asymptotic studies of the contact-shock ignition problem in [2, 6] and in the finite activation energy numerical simulations of the piston driven case examined in [5]. It is with these results which we wish to compare

8

the present results. However, we also briefly consider a case with $\gamma = 3$, in order to examine how the details of the evolution changes when a simple condensed phase equation of state model is used.

III. LARGE ACTIVATION ENERGY ASYMPTOTICS

In this section we briefly describe and examine the solutions obtained for the contact-shock ignition problem in the large activation energy asymptotic limit, $E \to \infty$ or $\epsilon = 1/E \to 0$, where ϵ is the inverse activation energy. In this limit the reaction history of a particle can be split into two main stages: an induction stage where the state remains within $O(\epsilon)$ of the initial state for an $O(1)$ timescale, followed by a main reaction or ignition stage where the burning proceeds to completion on an timescale which is exponentially short compared to the induction time [16]. Although the state changes by only $O(\epsilon)$ amounts during the induction phase, it is this weak reactive gas-dynamical evolution which determines the path of the supersonic reaction wave that emerges from the first point of ignition. The leading-order structure of the reaction wave itself is determined by the ignition stage [2].

The $O(\epsilon)$ induction stage solution is obtained via the expansions

$$T = 1 + \epsilon T_1 + O(\epsilon^2), \quad p = 1 + \epsilon p_1 + O(\epsilon^2), \quad \rho = 1 + \epsilon \rho_1 + O(\epsilon^2),$$

$$u = \epsilon u_1 + O(\epsilon^2), \quad \lambda = 1 + \epsilon \lambda_1 + O(\epsilon^2),$$

in the region between the contact surface and the shock. Inserting into Eqns. 1-5, one obtains Clarke's leading order induction equations [17], which in the scales used here are

$$\frac{\partial p_1}{\partial t} + \gamma \frac{\partial u_1}{\partial x} = \exp(T_1), \quad \frac{\partial u_1}{\partial t} + \frac{\partial p_1}{\partial x} = 0,$$

$$\frac{\partial T_1}{\partial t} - \frac{(\gamma - 1)}{\gamma} \frac{\partial p_1}{\partial t} = \frac{1}{\gamma} \exp(T_1), \quad \rho_1 = p_1 - T_1. \tag{7}$$

Equations 7 admit solutions which have local finite-time blow-ups of T_1 and p_1 ("thermal runaway"). These events signal the end of the induction stage for a particle and the onset of the exponentially short main reaction stage [1]. The time at which thermal runaway occurs is termed the induction time.

The initial conditions for Eqns. 7 correspond to the time at which the shock and contact surface are contiguous (e.g. the time at which the shock collision occurs in the shock merging

9

problem or the time the diaphragm bursts in the shock tube problem). For the problem of ignition between a contact surface and a shock, Eqns. 7 are subject to the linearized shock jump conditions at the shock front [6], together with the condition at the contact surface

$$u_{\text{contact}} = -\frac{p_{\text{contact}}}{\alpha_0},$$

which is derived from continuity of pressure and velocity across the contact surface together with a radiation condition [6]. Note that for the piston case, corresponding to the limit $\alpha_0 \rightarrow \infty$, this reduces to the condition $u = 0$. For an analysis correct to $O(\epsilon)$, these boundary conditions are applied on the leading order contact surface ($x = 0$) and shock ($x = M_0\sqrt{\gamma p_0 \rho_0}t$) paths [6].

Equations 7 are solved using the parametric integration method described in [2]. Here complete asymptotic solutions are obtained for a few cases which have not been characterized before. Only the solution for the case $\alpha_0 = 1.5$ was given in [2]. Also while Parkins [7] calculated some weak detonation paths using parametric variable integration described in Short & Dold [2], the weak detonation speeds (which are necessary for calculating the point of transition to strong detonation, see below) were not shown. Furthermore, much higher resolution is employed than was attainable for the calculations presented in [2, 7], an essential element to describing the path of the backward facing weak detonation.

Figure 1 shows the evolution of the temperature and pressure during the latter part of the induction stage for the gas phase model, with $\gamma = 1.4$, in the case $\alpha_0 = 0.5$ (chosen because low α_0 exemplifies the difference between the contact-shock problem from the piston driven case, cf [6]). During the early stages of rapid temperature growth, the temperature remains monotonically increasing as one moves back from the shock to the contact surface (particles nearer the contact surface have been shocked, and hence reacting and releasing heat, for the longest). However, the temperature maximum moves off the contact surface at $t = 1.31928$, which is only slightly before the initial blow-up time is reached. The reason for this is as follows. Throughout the induction stage, the gradient in fluid velocity, $\partial u/\partial x$, is positive and largest at the contact surface (the largest negative value of the fluid velocity occurs at the contact surface) [2]. As the induction time is approached and the rate of heat release begins to accelerate in the region ahead of the contact surface, the contact surface is driven backwards at an increasing rate and hence the fluid velocity gradient (or "rate of expansion") at the contact surface rapidly increases. A positive velocity gradient acts as a

10

local sink of thermal energy [18], and since it is largest at the contact surface, a competition between the rate of expansion and heat release occurs there, causing the temperature to begin to rise more rapidly in the interior than at the contact surface. Figure 1(a) shows that subsequently the temperature maximum continues to grow rapidly in an increasingly narrow boundary layer [6], indicating the onset of thermal runaway here. For $\alpha_0 = 0.5$, thermal runaway first occurs at time $t_0 = 1.3203$ at a distance of $x = 0.00125$ from the contact surface (cf the values of $t_0 = 1.186$, $x = 0$ for the piston case $\alpha_0 \to \infty$).

Meanwhile, Fig. 1(b) shows that even during the initial stages, the pressure is not monotonically increasing with distance behind the shock as occurs for the piston case, but instead has an internal maximum, due to acoustic pressure wave leakage at the contact surface. In fact for finite α_0, an early time analysis shows that initially the pressure *decreases* linearly with distance behind the shock, with gradient proportional to α_0^{-1} [6]. As runaway is approached the pressure maximum moves backward, and a finite time blow-up also occurs in p_1 at the same position as the temperature runaway [6]. Note, however, that both u_1 and ρ_1 remain bounded and monotonic [6].

As one moves away from this point of first runaway in either direction, particles will sequentially ignite at later times as they reach their induction times in turn. Thus two loci of thermal runaway times emerge from the initial point of ignition. It can be shown that the thermal runaway paths must move supersonically [1], through an essentially frozen induction region ahead of it. Thus Eqns. 7 can continue to be integrated in the regions ahead (in the direction of propagation) of the thermal runway loci and hence their paths determined. Since thermal runaway signals the onset of the ignition stage, one can associate a thermal runaway locus with the path of a vigorous reaction wave involving $O(1)$ variations in the material state through the wave. As the main reaction time and lengths are exponentially rapid in the asymptotic limit due to the Arrhenius form of the reaction rate, this wave will be quasi-steady to leading order, i.e. the timescale for a particle to traverse the reaction wave is much shorter than the timescale for changes in the wave's speed. In fact, it can be shown that the reaction wave takes the form of a quasi-steady weak detonation, i.e. a shockless compression wave which is supersonic throughout in the wave's rest frame [1, 2]. Consequently, the thermal runaway loci represent to leading order the paths of two weak detonations arising from the first point of thermal runaway. It is emphasized that in the contact-shock case, since ignition first occurs off the contact surface, both forward and

backward weak detonations move away from this point of initial runaway.

Note that here we do not describe the asymptotic structure of an initial rapid ignition transient: this is not explicitly needed for a description of the weak detonation path or structure [2], which is the the concern of the present paper. However, for the large activation limit, the structure of the initial ignition point could be described by the standard re-scaling analysis in [19]. Indeed, both Parkins [7] and Bauwens [9] have described the hot-spot structure for $\theta \to \infty$ and $(\gamma - 1) \to 0$. One would not expect qualitatively different results to the hot-spot structure when the second (Newtonian) limit approximation is dropped. However, this transient is not the concern of the present paper, which is focused on description of the weak detonation behaviour.

Figure 2 shows the weak detonation paths in the (x, t) plane for the case $\alpha_0 = 0.5$, as well as the magnitude of the inverse of the weak detonation speeds, $|v|^{-1}$. As can be seen, the forward and backward moving weak detonations emerge from the point of first thermal runaway at $x = 0.00125$, $t = t_0 = 1.3203$, with initially infinite speeds ($v^{-1} = 0$). However, the waves then decelerate rapidly as they move away. While the time scale for deceleration of the forward moving wave speed by an $O(1)$ amount is still very short, it decelerates more slowly than in the corresponding piston driven case ($\alpha_0 \to \infty$). On the other hand, the deceleration of the backward wave is extremely rapid. It can be shown that when, $\alpha_0 \leq 1$, this backward wave's speed asymptotes to $\sqrt{\gamma}$ (i.e. sonic) in the asymptotic or Newtonian limit $\gamma \to 1$ as it approaches the contact surface [7]. Nevertheless, despite this rapid deceleration, the wave reaches the contact surface at $t = t_0 + 1.82 \times 10^{-4}$, i.e. very soon after its formation.

A weak detonation only remains a valid structure whilst its speed remains above the Chapman-Jouguet (CJ) speed. Once the wave's speed drops to the CJ speed, D_{CJ}, the flow in the reaction burn-out region of the wave becomes sonic [1]. In the asymptotic scenario, this signals the birth of a secondary shock very near the rear of the wave, which rapidly accelerates through the remaining part of the weak detonation reaction zone ahead, trailing a fast-flame behind which couples with the secondary shock to form a strong detonation [1]. The transition from weak to strong detonation is exponentially rapid, so that the point at which the weak detonation speed reaches D_{CJ} effectively marks the point of strong

detonation formation. In the scalings used here, the CJ speed is given by

$$D_{\mathrm{CJ}}^2 = (\gamma^2 - 1)Q + \gamma + \left[(\gamma^2 - 1)Q((\gamma^2 - 1)Q + 2\gamma)\right]^{1/2}. \tag{8}$$

Note that the weak detonation path is independent of Q since it does not appear in Eqns. 7, but it does affect where the transition to strong detonation occurs. Equation 8 shows that the transition occurs earlier (where the weak detonation speed is higher) for larger Q. The CJ speed for $Q = 4$ is also shown in Fig. 2(b). For this value of Q, the transition point of the forward moving wave is at $x = 0.0128$. Again, while this is still a small distance, due to the slower deceleration of the forward wave, it is significantly larger than for the piston driven case where the transition occurs at $x = 0.002$ [5]. The transition point for the backward moving weak detonation, however, is 1.5×10^{-4}, i.e. the transition to strong detonation occurs virtually at the contact surface. The transition of the backwards wave occurs first, and very soon after ignition, at $t = t_0 + 1.1 \times 10^{-4}$, while the transition of the forward moving wave follows at $t = t_0 + 2.5 \times 10^{-3}$.

As α_0 increases, the thermal runaway time decreases (and approaches that in the piston driven case), but the length scales characteristic of the thermal runaway region also rapidly decrease. Figure 3 shows the weak detonation paths and speeds for the case $\alpha_0 = 1$. Thermal runaway first occurs at time $t_0 = 1.2840$, and at $x = 5.48 \times 10^{-4}$, i.e. about half the distance closer to the contact surface as for the $\alpha_0 = 0.5$ case. When $Q = 4$ and $\alpha_0 = 1$, the transition to strong detonation of the backwards moving weak detonation wave occurs earlier and even closer to the contact surface, at $t = t_0 + 4.7 \times 10^{-5}$, $x = 2.6 \times 10^{-5}$. The forward weak detonation wave also transitions earlier than in the $\alpha_0 = 0.5$ case, at $t = t_0 + 1.9 \times 10^{-3}$, $x = 0.0093$.

For an even larger value of $\alpha_0 = 2$, thermal runaway is found to occur at $t_0 = 1.2396$, $x = 1.61 \times 10^{-4}$, while the transition points occur at $t = t_0 + 1.06 \times 10^{-5}$, $x = 1.1 \times 10^{-6}$ and at $t = t_0 + 1.4 \times 10^{-3}$, $x = 0.0063$ for the backward and forward weak detonation waves, respectively. However, an important difference occurs when $\alpha_0 > 1$, in that the backward weak detonation no longer slows to the sound speed at the contact surface [2], hence transition to strong detonation is not guaranteed in these cases. For $\alpha_0 = 2$, $v = 3.16$ at the contact surface, which corresponds to $0.99 D_{\mathrm{CJ}}$ when $Q = 4$. For slightly smaller values of Q, the backwards weak detonation wave would not transition to strong detonation for this α_0, since then $D_{\mathrm{CJ}} < 3.16$.

Since the weak detonation decelerates extremely rapidly in these asymptotic solutions, the post-shock temperature scaled activation energy would need to be very high in order for the main reaction zone to be sufficiently thin such that the quasi-steady assumption in the asymptotic theory holds. Thus as in the piston case [4, 5], we expect that for moderately large finite activation energies the solutions will be qualitatively different to the asymptotic predictions, since the main reaction zone times will not short compared to the asymptotic wave deceleration time, and hence unsteadiness needs to be considered [5]. Furthermore, since the length and time-scales involved in the asymptotic become shorter as α_0 increases, larger activation energies can be expected to be required for the quasi-steady assumption to become valid.

Sharpe & Short [5] also described an interesting difference for the piston-shock case when a high polytropic index, more representative of condensed phase (liquid or solid) explosives [15] is used in the equation of state. In this case, the asymptotic evolution to detonation was found to be qualitatively different to those corresponding to gaseous values of γ. The weak detonation decelerated comparatively slowly, such that the transition point occurred at a distance of the order of unity from the piston face. This indicated that the quasi-steady assumption for the weak detonation should hold even for moderately large activation energies. Indeed finite E simulations showed that the asymptotic predictions were actually quantitatively good even for moderate E, in stark contrast to the gaseous equation of state cases.

Given this difference it is worth briefly considering how the induction phase and weak detonation behaves for a high polytropic index in the scenario of ignition between a contact surface and a shock in the limit of large activation energy. Figure 4 shows the induction stage solution when $\gamma = 3$ and $\alpha_0 = 0.5$. In this case, the temperature maximum moves off the contact surface comparatively much earlier, and thermal runaway first occurs at a relatively large distance from the contact surface. Ignition occurs at $t = t_0 = 1.9223$ and $x = 0.6018$, i.e. about three orders of magnitude more distant from the contact surface than for the $\gamma = 1.4$ case considered above.

The reasons for the large differences between the model condensed phase and gas phase cases can be understood by considering the temperature equation in Eqns. 7. In the limit $\gamma \to 1$, the evolution of T_1 decouples from the pressure evolution to leading order [7], and hence the leading-order rise in temperature is mainly due to the local self-acceleration of the

14

temperature induced by the heat release of the reaction, which is switched on by the passage of the shock. The rise in temperature is initially greatest at the contact surface where the material has been heated the longest. For $\gamma - 1 = O(1)$, however, the temperature evolution is also strongly coupled to the pressure evolution through the $((\gamma - 1)/\gamma) \partial p_1/\partial t$ material compressibility term. As for the gaseous γ cases considered above, the $\gamma = 3$ solution has an internal pressure maximum due to the acoustic leakage at the contact surface. The pressure maximum initially occurs at the shock, but grows and moves backward towards the contact surface. For $\gamma - 1 = O(1)$, localized increases in temperature occur not only via local heat release (which is initially largest at the contact surface where the material has been shocked the longest), but also due to localized increases in pressure, which are largest around the internal pressure maximum. Thus the growth of pressure internally has a much stronger role in determining the temperature profiles, and hence the first point of thermal runaway, when $\gamma = 3$ than for $\gamma = 1.4$. Figure 5 shows the weak detonation paths and speeds for the $\gamma = 3$ case. The forward moving weak detonation decelerates much more slowly than for the gaseous equation of state cases, as was also found for the piston scenario [5]. For $Q = 4$, the forward wave transitions to strong detonation at $x = 1.0426$, $t = 1.9508$ when $\alpha_0 = 0.5$, i.e. transition occurs a distance of 0.44 from the point of first thermal runaway, which is over twice the transition distance of 0.20 in the $\alpha_0 \to \infty$ case [5] when $\gamma = 3$. Figure 5(b) shows that the backward wave also decelerates relatively slowly: transition occurs at $x = 0.3320$, $t = 1.9371$ when $Q = 4$. The backward wave transitions first, at a distance of 0.27 from the point of first ignition. Thus, in contrast to the gaseous case, due to the magnified scales involved in the asymptotic solution for $\gamma = 3$ (e.g. the relatively slow evolution timescale of the weak detonations), one may expect that the quasi-steady structure will hold for the backward wave also even for moderate E. This prediction is also examined via the finite activation energy simulations in §IV.

Note that the results obtained by using a more realistic equation of state, $e(p, \rho)$, for condensed phase explosives should not be qualitatively different to those of the large polytropic index solutions. This is because the linearized equations resulting from a general equation of state are still of the same form as Eqns. 7, but with the polytropic index γ replaced by the constant c^2, where c is the dimensionless sound speed in the initial shocked state. Note that under our scalings, c^2 is, by definition, the value of adiabatic γ at the initial shock state. Hence $c^2 - 1$ is expected to be of the order of unity for condensed explosives,

and thus the solutions will be qualitatively similar to the large polytropic index results. If changes in the thermal equation of state, $T(p, \rho)$, are also taken into account, there will then be a difference in how temperature feeds into acoustic fluctuations. However, the resulting linearized equations are still of the same form as Eqns. 7.

IV. NUMERICAL SIMULATIONS FOR FINITE ACTIVATION ENERGY

In order to obtain the solutions for finite E, Eqns. 1-5 are solved numerically in the *AMRITA* computational environment [20, 21]. Adaptive mesh refinement is employed as described below. For accurate results it is important that the contact discontinuity is not smeared out by numerical diffusion such that its effective length becomes comparable to any other physical length-scales of the solution, as can readily occur with standard Eulerian shock capturing schemes [22]. Since potentially very short length-scales may appear in the ignition evolution for the current problem based on the asymptotic results in §III, the contact surface needs to be treated essentially as a discontinuity in the numerical solutions. To achieve this we utilize the mass-weighted Lagrangian second-order Godunov solver within the general equation of state *AMRITA* package described in [23]. The contact surface is then treated as a discontinuous material interface. However, for purposes of displaying the results, all solutions have been converted back into the more intuitive Eulerian (x, t) co-ordinates so as to clarify, for example, the movement of the contact surface, etc.

Our intention is to examine the generic problem of ignition between a contact surface and a shock, rather than a specific initial value problem which produces this configuration. Thus in the simulations, as in the asymptotic analysis, the initial conditions correspond to the time the shock and contact surface separate, i.e. to that of an initially stationary contact surface located at $x = 0$ with a shock of initial Mach number M_0 moving away from it $(x > 0)$ into a state ahead given by Eqns. 6. Behind the contact surface the initial conditions consist of the dimensionless constant state with $p = 1$, $u = 0$ and $\rho = \rho_B$ (so that $\alpha_0 = \sqrt{\rho_B}$). The left boundary of the numerical domain is placed sufficiently far behind the contact surface, such that no disturbances can reach it during the calculation period and hence is an inactive boundary. Similarly the right boundary of the domain is placed sufficiently far ahead that the initiating shock does not reach it.

In physical problems which may lead to this set-up, such as the shock merging or shock

16

tube scenarios, a backwards propagating expansion wave can also be produced behind the contact surface, which propagates away from the contact surface leaving behind a uniform state (in the inert case) between them where $\rho = \rho_B$, e.g. [6]. Since the rarefaction travels at the local sound speed, any acoustic disturbances originating in the reactively evolving induction zone ahead of the contact surface, which are subsequently transmitted into the region behind it, cannot catch up with this expansion wave. Thus the presence of the expansion will not affect our domain of interest and is not required as part of the calculation (note that this fact also underlies the formulation of the radiation condition at the contact surface in the large activation energy asymptotic solution [6]).

In the present simulations, the region behind the contact surface is taken to be inert. In the shock merging problem, for example, where it is guaranteed that $\alpha_0 > 1$, the material behind the contact surface would be reactive. In such problems though, it is assumed that the temperature behind the contact surface resulting from the shock merging is sufficiently low (based on a given E), that the characteristic ignition time is long (otherwise significant reaction would have occurred before the shock merging occurs). When the contact-shock complex is formed, the temperature behind the contact surface is lower than that behind the second shock before the merging, while both of these temperatures are lower than that between the contact surface and the shock. Consequently, for a sufficiently large E or α_0, to a first approximation, the reactivity of the material behind the contact surface can be ignored on the time-scale of the induction time in the region between contact surface and shock [6].

Even for the one-dimensional calculations, dynamical adaptive gridding is employed due to the large disparity between the induction length and time scales and those of the main reaction stage (these become exponentially disparate as the activation energy is increased). Resolution studies were performed to ensure that the solutions presented here are converged. The coarsest (base) grid, which covers the whole domain, is chosen to have a mesh spacing of 1000 points per unit length based on the initial shocked state. Dynamic grid refinement levels are then defined in regions when and where they are required. The Lagrangian mesh spacing is reduced by a factor of four on each subsequent grid level. The induction region between the contact surface (inclusive) and the shock is always covered by the first refinement level. Subsequent to the end of the induction stage, a finer mesh spacing may be necessary to resolve the more rapid main reaction stage. Hence the grid is also refined based on local

pressure gradients, up to a grid refinement level N, say, which depends on the activation energy. The most stringent condition on the resolution is to resolve the secondary shock in the $p\lambda$ plane (see below) subsequent to its formation, i.e. to ensure there is no burning within the captured secondary shock structure. More refinement grids (larger N) are required as the activation energy is increased. The initiating shock is always resolved on the finest grid level defined to ensure that this captured shock remains appropriately narrow compared to any physical length-scale of the problem. Also, in the initial conditions the shock is placed one grid point of this finest grid level ahead of the contact surface. To ensure the length-scales associated with the numerical shock are small compared to any of the physical scales, a minimum of least five refinement levels are defined.

As E increases, it rapidly becomes difficult to resolve (in both space and time) the main reaction stage, and the problem becomes very stiff, due to the exponential shortening of the characteristic main reaction length and time scales (see the discussion in [5]). Furthermore, as E increases, local induction times become sensitive to decreasingly small perturbations in the temperature history. As $\epsilon = 1/E \to 0$, $O(\epsilon)$ perturbations in the temperature produce $O(1)$ changes in the induction times [18]. Hence as E increases, even very small amounts of numerical noise can be amplified during the induction stage, rendering it very difficult to obtain highly accurate solutions. Analogously, in experiments, when the temperature sensitivity of the fuel becomes sufficiently large, ignition no longer occurs along a one-dimensional locus, but thermal runaways occur at discrete isolated points (resulting in so called 'mild ignition') due to the amplification of small inhomogeneities in the fuel or geometry [24], hence producing a three-dimensional problem. For the above numerical reasons, the simulations of the full evolution are hence limited to cases $E \leq 20$ as in [5] for the piston driven case, while the initial stages of the evolution are also consider for somewhat larger values of E in order to demonstrate the trends as E increases. Indeed, the purpose of the simulations is precisely to contrast these moderately large finite activation energy solutions with the asymptotic prediction, and not an attempt to recover the asymptotics solutions.

At this point, it is worth comparing the values of E used in the simulations with representative values for fuels which may be described, at least to a first approximation, by a one-step Arrhenius rate, i.e. those for which the chemical heat release is characterised by a weak heat release induction zone, terminated by a much more rapid thermal explosion. Examples include methane, propane and ethane mixtures with oxygen [25, 26] and hydrogen-

oxygen-diluent mixtures at initial temperatures below the chain-branching crossover temperature, where chain-recombination is dominant over chain-branching [25, 26]. Note that an analysis of constant volume explosions in a generic three-step chain-branching model (which includes chain-initiation, -branching and -recombination steps) shows that, for initial temperatures sufficiently below the crossover temperature, the heat release rate and hence temperature evolution does indeed effectively reduce to that of an overall one-step model [27, 28]. Furthermore, the one-step model then also recovers the shock ignition dynamics of the chain-branching model when the initial shock temperature is below that of the cross-over temperature [28].

Note that, for a given mixture, the effective (shock temperature scaled) activation energy, E, will depend intimately on the initial shock strength. Values of E at different initial temperatures ($> 1000K$) and pressures were found by considering changes of the constant volume explosion induction time with temperature [25], giving $E \sim 15$ for methane-oxygen, $\sim 15 - 25$ for ethane-oxygen, and $\sim 20 - 25$ for hydrogen-oxygen-diluent mixtures in the region below the cross-over temperature. The induction time data given in [26] also indicates that an upper bound for E is 20 for methane-oxygen, 18 for propane-oxygen, and 25 for hydrogen-air, for initial temperatures greater than $\sim$1000K.

In order to interpret the results of the simulations we use the diagnostic methods described in [29], which involve plotting the solutions in the pressure-specific volume, pV, and pressure concentration, $p\lambda$, planes. These pV and $p\lambda$ diagrams allow one to identify components of quasi-steady reaction waves, induction zones, unsteady combustion zones and burnt regions in the solution, as well as where these various features occur [4, 5, 29].

A. Results

We consider first the case $\alpha_0 = 0.5$. Recall that for this value of α_0, in the high activation energy asymptotic limit, thermal runaway occurs first at $x = 0.00125$ and $t = 1.3203$, while the backward and forward weak detonation waves transition to strong detonation at 9×10^{-5} and $x = 0.013$, respectively (Fig. 2).

Figure 6 shows the initial evolution during the induction phase for $E = 15$. For the finite activation energy cases, we will define the induction phase as lasting until the time when λ reaches 0.5 at the contact surface. During this stage when $E = 15$, the temperature

and reaction progress variable profiles remain monotonically increasing as one moves back from the shock to the contact surface, as in the finite activation energy piston driven shock scenario. Note, however, that the contact surface has been pushed backwards (relative to its position at any given time in the corresponding non-reactive case) due to the reaction induced thermal expansion ahead of it. The temperature maximum remains at the contact surface, even up to the point when half the fuel is consumed there. This is in contrast to the asymptotic prediction that rapid burning first occurs a small distance ahead of the contact surface.

Figure 7 shows the later time evolution for $E = 15$. At the the first time shown, corresponding to $t = 1.693$, the temperature maximum has now moved ahead of the contact surface. The pressure profiles also indicate that the pressure maximum has begun to move forward again. While the temperature maximum does move into the interior region between the contact surface and the shock for $E = 15$, it only does so once the fuel is largely consumed there, specifically $\lambda = 0.85$ in the region near the temperature maximum at the time it moves off the contact surface. This is in contrast to the movement of the temperature maximum off the contact surface during the $O(\epsilon)$ induction phase evolution that occurs in the large activation energy limit. Indeed, the progression of the temperature maximum away from the contact surface only occurs for $E = 15$ since the rate of heat release is diminishing at the contact surface due to the near total consumption of fuel there.

At the second time shown in Fig. 7, the fuel near the contact surface has fully depleted, and the temperature and pressure maxima have moved further forward towards the shock, with the location of the maximum in the temperature beginning to catch up with that in the pressure. Subsequent profiles show the emergence and propagation of a reaction wave structure. This is clearly shown in the pV diagrams (Fig. 7c), which reveal that as one moves back from the shock various different reaction regimes begin to arise. Initially following the shock is a region which has positive slope in the pV plane, representing an unsteady induction region. This is followed by a region through which pressure increases along an approximately straight line in the pV plane with negative slope. This region of the solution thus constitutes part of a quasi-steady, supersonic weak detonation [29]. As was also found in the finite activation energy numerical simulations of the piston-shock scenario [5], this wave-like behaviour does not begin at the point where reactions first became rapid. Instead, Fig. 7 shows that it takes a finite time for the weak detonation to form: the slope

of the pV trajectories inside the reaction zone complex only become negative between the second and third times ($t = 1.715$ and $t = 1.737$) shown in Fig. 7(c). The quasi-steady weak detonation regime thus emerges in the region $x > 0$ in Fig. 7(b), at which time the contact is at $x = -0.08$. This is in contrast to the large activation energy asymptotic solution in both cases, where weak detonations effectively originate at the point of first thermal runaway (e.g. at the piston face ($x = 0$) in the limit $\alpha_0 \to \infty$).

As time progresses, the magnitude of the slope corresponding to the weak detonation regime decreases in Fig. 7, showing that the weak detonation part of the reaction structure is decelerating [29]. The weak detonation regime is in turn followed by highly curved, and hence highly unsteady [29], reaction regime in the pV plane. The final part of the reaction zone lies within a second region of negative slope through which the pressure decreases, which thus constitutes a subsonic fast-flame regime[29]. An expansion wave in the fully burnt material then connects the rear of the reaction zone to the contact surface (Fig. 7a). The reaction wave complex moves towards the shock. A backward (toward the contact surface) propagating reaction complex does not form, in contrast to the asymptotic solutions described in §III.

The $p\lambda$ trajectories in Fig. 7(d) show that at the beginning of the reaction wave complex propagation stage, the pressure maximum occurs near the fully burnt state ($\lambda \approx 0.95$ there), so that the bulk of the reaction wave comprises of the weak detonation regime. As the pressure maximum begins to move forward through the reaction zone complex, both the unsteady and fast-flame parts of the wave structure become more pronounced. The pressure profile ahead of the maximum also begins to rapidly steepen. This steepening results in the formation of a weak interior shock, which occurs at $t = 1.775$ and can be observed at the last time shown in Fig. 7(d). The secondary shock forms at $x = 0.23$, in poor agreement with the asymptotic prediction of the point of slowing to the CJ detonation speed, $x = 0.013$, for the forward moving weak detonation wave.

The above evolution for $\alpha_0 = 0.5$, $E = 15$, involving the emergence of a single, forward moving, unsteady reaction wave complex, is qualitatively similar to the piston driven shock initiation evolution with the same activation energy described in [5]. For a more direct comparison, the loci of the shock pressure maximum from the piston driven case with $E = 15$ [5] are also shown in Fig. 7(b-d). Figure 7(b) shows that spatially the growth of the pressure is slower for $\alpha_0 = 0.5$ compared to the $\alpha_0 \to \infty$ solution. In terms of the evolution in the pV

and $p\lambda$ planes, however, the two cases are similar. The pressure maximum for $\alpha_0 = 0.5$ lies only slightly behind that of the piston case, indicating that both cases have similar extents of a quasi-steady weak detonation structure in the $p\lambda$ plane [5]. The point of formation of the secondary shock also occurs at almost the same degree of reaction within the wave, cf [5]. The evolution for $E = 15$ subsequent to that shown in figure 7, including the mechanism of strong detonation formation, is also similar to that for the piston case when $E = 15$ as described in [5].

In order to examine how the solution depends on the activation energy, its value was increased to $E = 20$, keeping $\alpha_0 = 0.5$. The evolution for this case is shown in Figs. 8 to 10. Figure 8 shows the induction stage evolution (up to the point where λ approaches 0.5 at the contact surface). The initial evolution is similar to that for $E = 15$ above (cf Fig. 6), except now the region of initial rapid temperature rise occurs in a narrower layer close to the contact surface.

The main difference with the $E = 15$ case considered above is that a definite interior local maximum in temperature forms, at an earlier stage. This is revealed in Fig. 9, which shows a zoomed-in view of the spatial profiles near the contact surface, between times 1.555 and 1.562. Figure 9(a) and (c) show that the temperature maximum begins to move ahead of the contact surface when $\lambda \approx 0.4$ there, as compared to $\lambda = 0.85$ for the $E = 15$ case. The temperature maximum also remains close to the contact surface, and becomes more pronounced, during the initial self-acceleration of the temperature rise. For example, at $t = 1.562$ in Fig. 9, the temperature maximum occurs at $x = -0.027$ as compared to the contact surface location of $x = -0.036$. The pressure maximum (located at $x = -0.026$ when $t = 1.562$) can also be seen to occur close to where the temperature takes its maximum. The evolution for $E = 20$ is thus in better agreement with the prediction of the asymptotics than that for $E = 15$. Note from Fig. 9 that, as the temperature begins to move ahead of the contact surface, λ initially remains monotonic, but subsequently an interior maximum in λ also forms, which lags very slightly behind that in the temperature.

Figure 10 shows the later time evolution. The interior maxima in p and λ result in a "hook" in the $p\lambda$ diagrams (Fig. 10d) at the first two times shown. Thus at these times there exists a compressive (in the direction of increasing reaction progress) region between the contact surface and the pressure maximum. This region hence has negative slope in the pV diagram (Fig. 10c). However, the reaction rates both at the contact surface and

at the temperature maximum are not substantially different at these times, so that the material in this entire region rapidly burns out subsequent to the time where λ first reaches unity. Consequently this compressive region quickly disappears from the $p\lambda$ plane (e.g. by the third time shown in Fig. 10d). In contrast, we recall that in the large activation energy asymptotic scenario, the material remains virtually frozen at the contact surface while runaway to complete reaction occurs at the temperature maximum. Thus, despite the appearance of the internal maximum, the reactive evolution of the region between the contact surface and the temperature maximum for $E = 20$ is again different to that predicted by the large activation energy scenario. The pV diagrams in Fig. 10(c) show that a forward moving weak detonation only begins to form (when the slope of the pV trajectories corresponding to the region ahead of the pressure maximum becoming negative) subsequent to the complete burnout of the fuel between the contact surface and the temperature maximum. Again, a backwards moving reaction wave does not emerge.

The pV and $p\lambda$ diagrams in Fig. 10(c,d) show that subsequently almost the entire reaction zone complex consists of a weak detonation, with the pressure maximum occurring close to $\lambda = 1$. Thus, as in the piston driven case [5], the quasi-steady weak detonation structure is more readily apparent throughout the reaction zone when $E = 20$ than when $E = 15$. This occurs due to the shortening of the main reaction zone length and time scales relative to the induction zone scales. For comparison, the loci of the pressure maximum for the corresponding piston case is also shown in Fig. 10. The pV and $p\lambda$ evolutions are again in quantitative agreement with the piston driven case, e.g. the locus of the pressure maximum for $\alpha_0 = 0.5$ lies only slightly ahead of that for $\alpha_0 \to \infty$ in the $p\lambda$ plane. The secondary shock forms at $x = 0.056$, corresponding to a distance of 0.102 from the contact surface which is at $x = -0.046$ at the time of the interior shock formation. Compare this with the shock formation distance from the piston face of 0.037 in the piston driven shock solution for $E = 20$ [5]. Hence, when $E = 20$, as for the $E = 15$ case, the evolution to detonation for the contact-shock problem is similar to that in the piston driven case.

Figure 11 shows the formation of the internal temperature maximum for $E = 22$ and $E = 23$, which further illustrates the trends as the activation energy is increased. The temperature maximum moves off the contact surface earlier, at a smaller value of λ, as E increases, while the position of the maximum during the initial self-accelerating temperature rise occurs closer to the contact surface. The peak of the temperature maximum also becomes

more pronounced, in that differences between the temperatures at the contact surface and at the maximum become more disparate as E increases. The distances from the contact surface to the maximum at the last times shown in figure 11(a) and (b) are 0.006 and 0.005 for $E = 22$ and $E = 23$, respectively.

Figure 12 shows a subsequent stage of the evolution for $E = 22$. Initially, the compressive reaction region between the contact surface and the pressure maximum is much more pronounced in both the pV and $p\lambda$ diagrams than for $E = 20$. It is seen that this whole region still reacts rapidly, and hence the state at the contact surface again does not remain frozen during the first interior ignition event, as occurs in the asymptotic solution. However, the reaction rates at the temperature maximum and at the contact surface are now more disparate (note the much larger change in the maximum values of p and λ over the first two times shown in Fig. 12d as compared to the change in their values at the contact surface). Hence a partially reacted region near the contact surface remains in evidence while the material immediately around the temperature maximum burns out. Nevertheless, Fig. 12(c) shows that the material at the contact surface burns out before the forward moving weak detonation forms (at fourth time shown in Fig. 12).

Figures 13 and 14 shows the effect of α_0 for a fixed activation energy of $E = 15$. When $\alpha_0 = 1$ (Fig. 13) the ignition time is less than that for the $\alpha_0 = 0.5$ case, in agreement with the asymptotic prediction that the thermal runaway time is longer for lower α_0. However, the spatial evolution between the contact surface and the shock wave is still similar to that shown in Fig. 7(a,b) for $\alpha_0 = 0.5$. The pressure peak grows slightly faster for the larger value of α_0, and the deceleration of the contact surface is less due to the larger acoustic impedance of the material behind it. The solution shown in Fig. 14, which corresponds to $\alpha_0 = 2$, reveals that these trends continue as α_0 is increased further. For example, the timing of events further approach those of the piston case. Figures 13 and 14 together with the piston driven shock results in [5] show that, in contrast to the asymptotic solutions examined in §III, there is only a weak dependence of the evolution sequence on α_0 as it is varies from low values to infinity when $E = 15$. The pV and $p\lambda$ evolutions are not shown for $\alpha_0 = 1$ and 2 as they are quantitatively similar to those for the $\alpha_0 = 0.5$ case shown in Fig. 7(c,d).

For the final case, we briefly consider a finite activation energy solution for the simple condensed phase equation of state assuming $\gamma = 3$. In this case the large activation energy

asymptotic solution revealed that a high polytropic index produces a qualitative change in the evolution scenario compared to that for values of γ appropriate for the gas phase. Figure 15 shows the evolution of the induction phase (defined here as up to the time when λ first reaches 0.5) for the case $E = 15$, $\gamma = 3$, $\alpha_0 = 0.5$. Here, as predicted by the large E asymptotic description, an internal temperature maximum develops at a distance of order unity away from the contact surface as the temperature rise begins to self-accelerate. The temperature maximum is located at $x = 0.74$ in Fig. 15(a), compared to $x = 0.60$ in the asymptotic solution for $\alpha_0 = 0.5$ (Fig. 4). Furthermore, the degree of reaction at the contact surface remains small while the first ignition event occurs around the region of the interior temperature maximum, again in contrast to the finite activation energy solutions for values of γ appropriate to gases as described above. In this case, a backward moving reaction wave complex now has time to develop in the region between the contact surface and temperature maximum before the material near the contact surface burns to completion.

Figure 16 and 17 show the evolution subsequent to the first ignition event, which reveal that both forward and backward moving reaction waves do indeed emerge. Figure 16 shows spatial temperature and pressure profiles, from which it can be seen that the amplitude of the backward reaction wave complex grows more rapidly than the amplitude of the forward wave. Figure 17 shows pV and $p\lambda$ trajectories at various times to clarify the evolutionary mechanisms of these wave. At $t = 2.252$, the diagrams show that several regimes exist as one moves back from the initiating shock to the contact surface. Between the shock and the forward moving reaction wave is an unsteady induction region, through which the forward wave is moving. This wave can be seen to consist almost entirely of a quasi-steady weak detonation as predicted by the asymptotic theory, and is followed by an inert expansion wave ($\lambda = 1$ in the expansion subsequent to the pressure maxima according to Fig. 17b). This is in turn followed by a backward moving inert expansion wave, which in turn trails a backward moving reaction wave. The backward reaction wave again consists of an almost complete quasi-steady weak detonation. Finally, another unsteady induction region exists between the contact surface and the backward moving reaction wave.

At the second time shown in Fig. 17, the pV diagrams reveal that the backward moving reaction wave is decelerating more rapidly than the forward moving wave (its slope decreases faster in the pV plane), again in agreement with the large activation energy asymptotic prediction. In fact, Fig. 17(d) shows that a secondary shock is about to form near the rear

25

of the backward wave. This secondary shock forms at $x = 0.30$, in quantitative agreement with the value of $x = 0.33$ obtain in the limit $E \to \infty$. By the third time shown in Fig. 17, this secondary shock and following fast-flame in the backward wave have become a fully coupled quasi-steady strong detonation (they lie along a common straight line in the pV plane [29]). Meanwhile, at this time, a secondary shock has now begun to form at the rear of the forward moving wave. The secondary shock for this wave occurs at $x = 1.41$, again in good agreement with the large activation energy asymptotic prediction of $x = 1.04$.

In conclusion, as found for the piston case [5], while the asymptotic and finite activation energy solutions show qualitative differences when polytropic indices representative of gaseous fuels are used, for large values of γ as employed in simple condensed phase models, the finite activation energy solutions agree quantitatively well with the asymptotic predictions even for only moderately large values of E, due to the much slower deceleration of the the weak detonations.

V.   CONCLUSIONS

In this paper, the events which lead to ignition and detonation formation of reactive materials in the region between a contact surface and a shock were examined using both high activation energy asymptotics and finite activation energy direct numerical simulations. For a polytropic index appropriate to gaseous explosives, the large activation energy asymptotic solutions differ from those of the problem of ignition between a piston and a shock wave, in that thermal runaway first occurs off (but still very close to) the contact surface, and hence both forward and backward quasi-steady weak detonations subsequently emerge. Both weak detonations may subsequently transition to strong detonation. In the finite activation energy simulations, however, the solutions are qualitatively different from these asymptotic predictions, in that while the temperature maximum may move off the contact surface before burning is complete there, only a forward moving reaction wave emerges. For finite activation energies, only a weak dependence on the acoustic impedance of the material behind the contact surface is found, such that the sequence of events leading up to detonation initiation between the contact surface and shock wave are actually described quite well by the piston driven solution. The differences between the asymptotic theory and the numerical results arise due to the exponentially short reaction times of a particle traversing the weak

26

detonation as compared to it evolution timescale (hence its quasi-steady structure) that occur in the large activation energy limit. Such short reaction times are not reproduced for finite activation energies considered.

For a polytropic index appropriate to a simple condensed phase model, the results are qualitatively different to those described above. In the large activation energy asymptotic limit, thermal runaway now occurs at a distance of order unity from the contact surface due to the stronger coupling of the temperature evolution with localized rises in pressure. Both the forward and backward moving weak detonations which emerge from this first point of ignition decelerate more slowly than in the gas phase cases. Due to the slower rate of deceleration, the large activation energy asymptotic description remains valid over longer length and time scales, and consequently the finite activation energy solutions are found to agree quantitatively with the asymptotic predictions, even for only moderately large activation energies.

Previously, it has been shown that the ignition mechanisms may be qualitatively different for reactive materials whose kinetics are not well described by the one-step chemistry model [28, 30–33]. These include, for example, cases where the initial temperature is above a chain-branching cross-over temperature, whence chain-branching is dominant over chain-recombination [28, 33]. Simple models appropriate to this regime, entailing a mainly chain-branching explosion rather than a thermal explosion as examined here, show that a subsonic reaction wave emerges in the piston driven shock initiation solutions [28, 30, 31, 33]. A preliminary examination of the contact-shock initiation solutions for these simple chain-branching models indicate that this remains the case for when the piston is replaced by a contact surface. For models with thermally neutral induction stages, the main reaction stage begin at the contact surface both in the large activation energy limit and for finite activation energies [33]. Hence the results in [33] indicate that for these kinetic models, there is only a weak dependence of the evolutionary events on the acoustic impedance behind the contact surface in both cases. We intend to examine the solutions for different kinetic models more thoroughly in the future, in order to compare with the one-step results presented here.

Acknowledgments

---

[1] A. K. Kapila and J. W. Dold, "A theoretical picture of shock-to-detonation transition in a homogeneous explosive," Ninth Symposium (International) on Detonation, 219 (1989).

[2] M. Short and J. W. Dold, "Weak detonations, their paths and transition to strong detonation," Combust. Theory Model. **6**, 279 (2002).

[3] J.W. Dold, "Emergence of a detonation within a reacting medium". In *Fluid dynamical aspects of combustion theory* (Eds M. Onofri and A Tesei) London: Longman pp. 161–183.

[4] G. Singh and J. F. Clarke, "Transient phenomena in the initiation of a mechanically driven plane detonation," Proc. Roy. Soc. Lond. A, **438**, 23 (1992).

[5] G. J. Sharpe and M. Short, "Shock-induced ignition of thermally sensitive explosives," IMA J. Appl. Math. **69**, 493 (2004).

[6] M. Short and J. W. Dold, "Unsteady gasdynamical evolution of an induction domain between a contact surface and a shock wave: I: Thermal runaway" SIAM J. Appl. Math. **5**, 1295 (1996).

[7] C. J. Parkins, "Shock-generated ignition. Newtonian asymptotics for the induction domain between a contact surface and shock," SIAM J. Appl. Math. **61**, 701 (2000).

[8] P. A. Urtiew and A. K. Oppenheim, "Detonative ignition induced by shock merging," Proc. Combust. Inst. **11**, 665 (1966).

[9] L. Bauwens, "Ignition between a shock and a contact surface: Influence of the downstream temperature,", Proc. Combust. Inst. **28**, 653 (2000).

[10] S. A. Sheffield, R. L. Gustavsen, L. G. Hill, R. Engelke, R. R. Alcon and L. L. Davis, "In-situ study of the chemically driven flow fields in initiating homogeneous and heterogeneous Nitromethane explosives," Ninth Symposium (International) on Detonation, 39 (1989).

[11] R. L. Gustavsen, S. A. Sheffield, R. R. Alcon, R. R. Forbes, C. M. Tarver and F. Garcie, "Embedded electromagnetic gauge measurements and modelling of shock initiation in the TATB based explosives LX-17 and PBX 9502", in: *Shock Compression of Condensed Matter*, edited by M. D. Furnish, N. N. Thadhani and Y. Horie (American Institute of Physics), 1012, (2001)

[12] K. Kailasanth and E. S. Oran, "Ignition of flamelets behind incident shock waves and transition to detonation," Combust. Sci. Tech. **34**, 345 (1983).

[13] L. Bauwens, D. N. Williams and M. Nikolic, "Failure and reignition of one-dimensional detonations - the high activation energy limit," Proc. Combust. Inst. **27**, 2319 (1998).

[14] S. Taki and T. Fujiwara, "One-dimensional nonsteady process accompanied by the establishment of self-sustained detonation," Proc. Combust. Inst. **13**, 1119 (1971).

[15] W. Fickett and W. C. Davis, *Detonation.* (University of California Press, Berkeley, 1979).

[16] A. K. Kapila, *Asymptotic treatment of chemically reacting systems.* (Pitman, Boston, 1983).

[17] J. F. Clarke, "Propagation of gasdynamic disturbances in an explosive atmosphere," Prog. Astron. Aeron. **76**, 383 (1981).

[18] M. Short, "Homogeneous thermal explosion in a compressible atmosphere," Proc. R. Soc. Lond. A **452**, 1127 (1996).

[19] T. L. Jackson, A. K. Kapila and D. S. Stewart, "Evolution of a reaction center in an explosive material," SIAM J. App. Math. **49**, 432 (1989).

[20] J. J. Quirk, "Amrita - a computational facility for CFD modelling", in: *29th Computational Fluid Dynamics VKI Lecture Series*, edited H. Deconinck (von Karmen Institute). ISSN0377-8312. (1998)

[21] J. J. Quirk, "AMR_sol: design principles and practice", in: *29th Computational Fluid Dynamics VKI Lecture Series*, edited H. Deconinck (von Karmen Institute). ISSN0377-8312. (1998)

[22] C. B. Laney, *Computational Gasdynamics.* (Cambridge University Press, Cambridge, 1998).

[23] R. Menikoff and J. J. Quirk, "Versatile user-friendly EOS package," Los Alamos National Laboratory Technical Report, LA-UR-01-6222 (Los Alamos), 2001.

[24] J. W. Meyer and A. K. Oppenheim, "On the shock-induced ignition of explosive gases," Proc. Combust. Inst. **13**, 1153 (1971).

[25] J. E. Shepherd personal communication, 2007, and presented at the Proceedings of the Fall
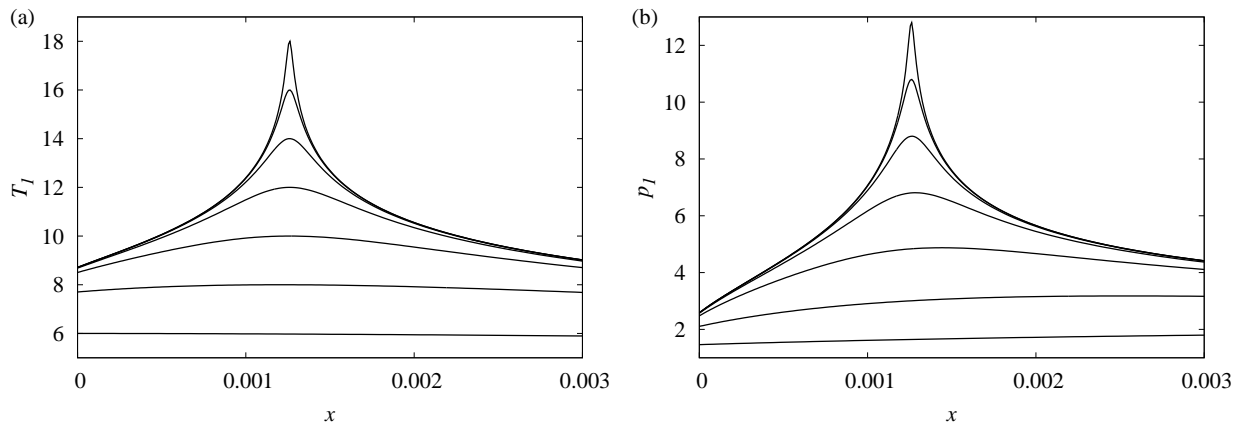
FIG. 1: Evolution of (a) temperature perturbation, T_1, and (b) pressure perturbation, p_1, close to the contact surface during the large activation energy asymptotic induction stage when $\alpha_0 = 0.5$ at times $t = t_0 - 2.89 \times 10^{-3}$, $t_0 - 3.48 \times 10^{-4}$, $t_0 - 4.57 \times 10^{-5}$, $t_0 - 6.15 \times 10^{-6}$, $t_0 - 8.32 \times 10^{-7}$, $t_0 - 1.14 \times 10^{-7}$ and $t_0 - 1.7 \times 10^{-8}$, where $t_0 = 1.32027$ is the thermal runaway time.

Western States Section of the Combustion Institute as Paper 05F-21, 2005.

[26] M. I. Radulescu, "The propagation and failure mechanism of gaseous detonations: experiments in porous-walled tubes," PhD thesis,McGill University, Montreal, Canada (2003).

[27] P. A. Blythe, A. K. Kapila and M. Short, "Homogeneous ignition for a three-step chain-branching reaction model," J. Eng. Math **56**, 105 (2006).

[28] G. J. Sharpe and N. Maflahi, "Homogeneous explosion and shock initiation for a three-step chain-branching model," J. Fluid Mech., **566**, 163 (2006).

[29] J. F. Clarke and N. Nikiforakis, "Remarks on diffusionless combustion," Phil. Trans. R. Soc. Lond. A **357**, 3605 (1999).

[30] J. W. Dold and A. K. Kapila, "Comparison between shock initiations of detonation using thermally-sensitive and chain-branching chemistry model," Combust. Flame **85**, 185 (1991).

[31] G. J. Sharpe, "Shock induced ignition for a two-step chain-branching kinetics model," Phys. Fluids **14**, 4372 (2002).

[32] G. J. Sharpe and M. Short, "Detonation ignition from a temperature gradient for a two-step chain-branching kinetics model," J. Fluid Mech. **447**, 31 (2002).

[33] N. Maflahi, "Theory of explosions and detonations for a three-step chain-branching chemistry model," PhD thesis, University of Birmingham, Birmingham, UK (2005).
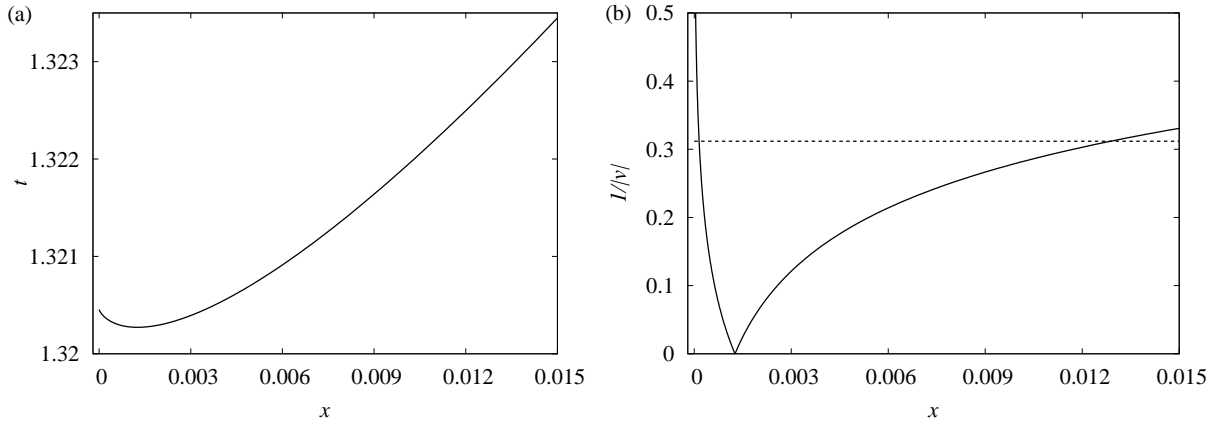
FIG. 2: (a) Path of weak detonations in the (x, t) plane and (b) magnitude of the inverse of the weak detonations' speeds, in the large activation energy asymptotic solution when $\alpha_0 = 0.5$. Also shown as the dotted line is the CJ speed for $Q = 4$.
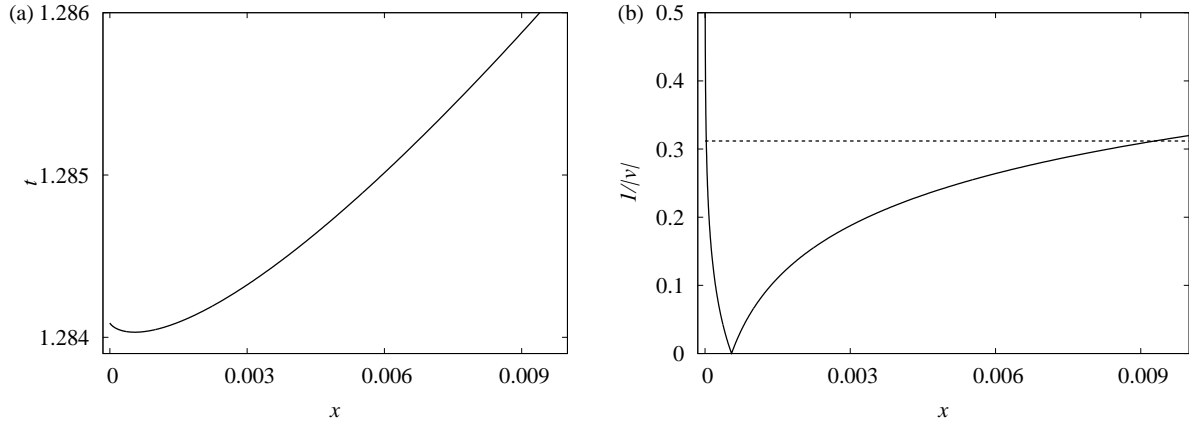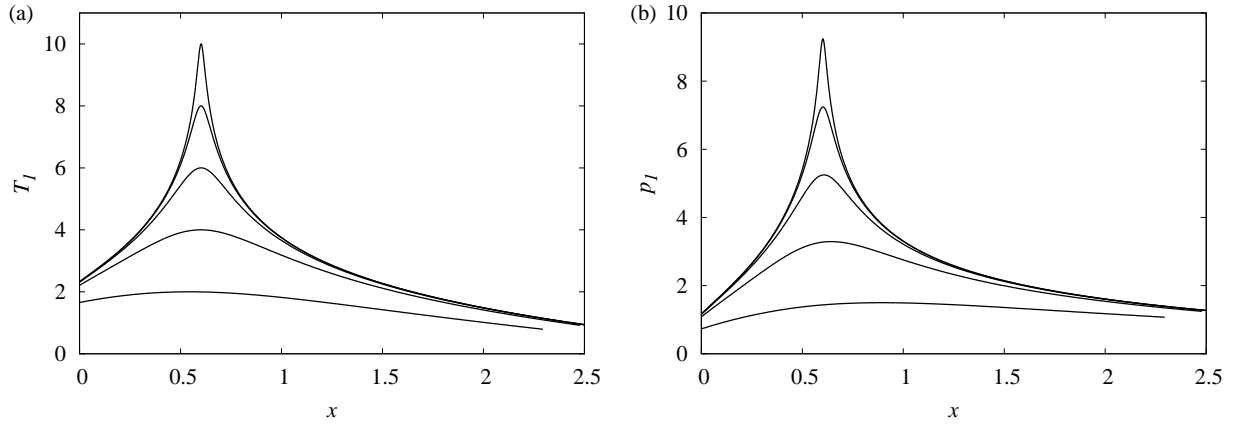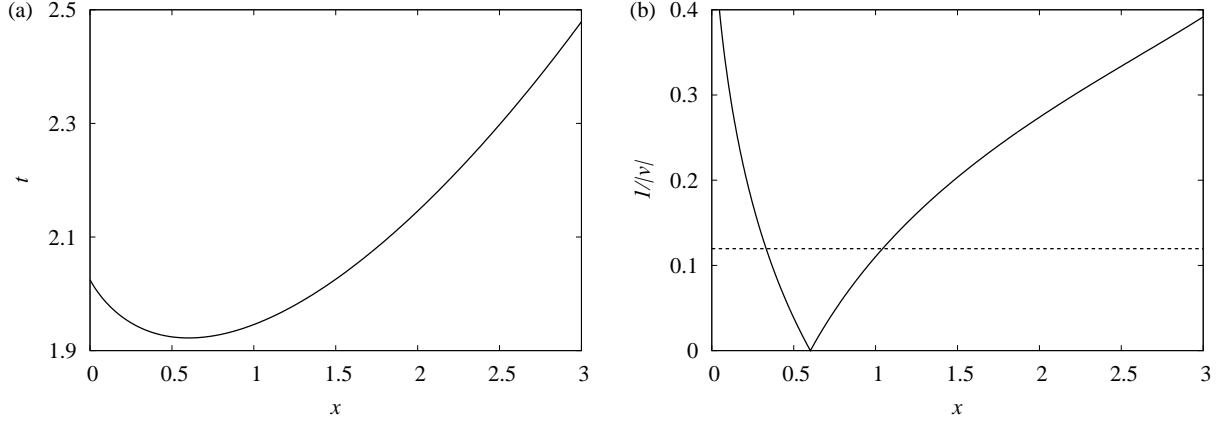

FIG. 3: (a) Path of weak detonations in the (x, t) plane and (b) magnitude of the inverse of the weak detonations' speeds, in the large activation energy asymptotic solution when $\alpha_0 = 1$. Also shown as the dotted line is the CJ speed for $Q = 4$.

FIG. 4: Evolution of (a) temperature perturbation, T_1, and (b) pressure perturbation, p_1, during the large activation energy asymptotic induction stage when $\alpha_0 = 0.5$ and $\gamma = 3$ at times $t = 1.7620$, 1.9034, $t_0 - 2.49 \times 10^{-3}$, $t_0 - 3.36 \times 10^{-4}$ and $t_0 - 4.54 \times 10^{-5}$, where $t_0 = 1.92232$ is the thermal runaway time.

FIG. 5: (a) Path of weak detonations in the (x, t) plane and (b) magnitude of the inverse of the weak detonations' speeds, in the large activation energy asymptotic solution when $\alpha_0 = 0.5$ and $\gamma = 3$. Also shown as the dotted line is the CJ speed for $Q = 4$.

32
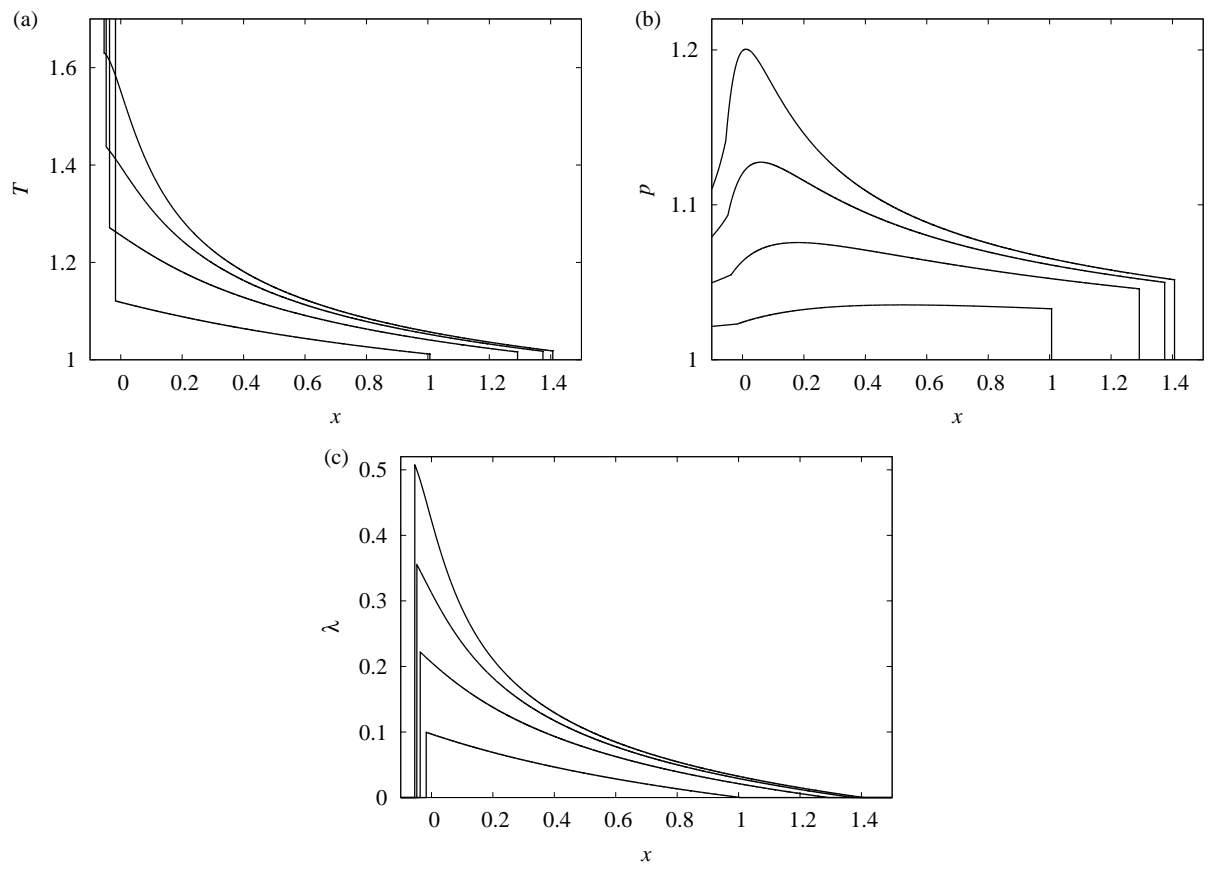
FIG. 6: Spatial profiles of (a) temperature, (b) pressure and (c) reaction progress variable, for $E = 15$ and $\alpha_0 = 0.5$, at times $t = 1.197$, 1.530, 1.626 and 1.663.
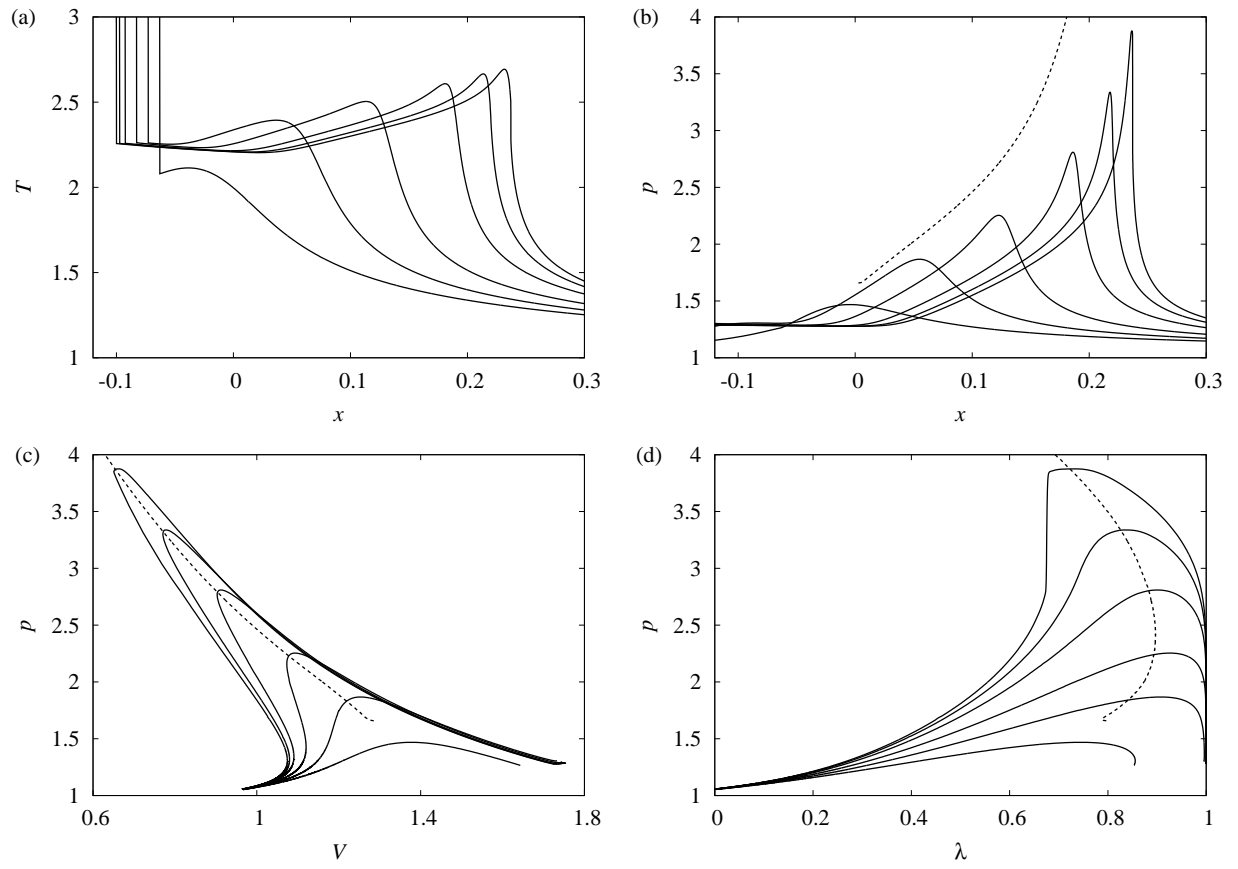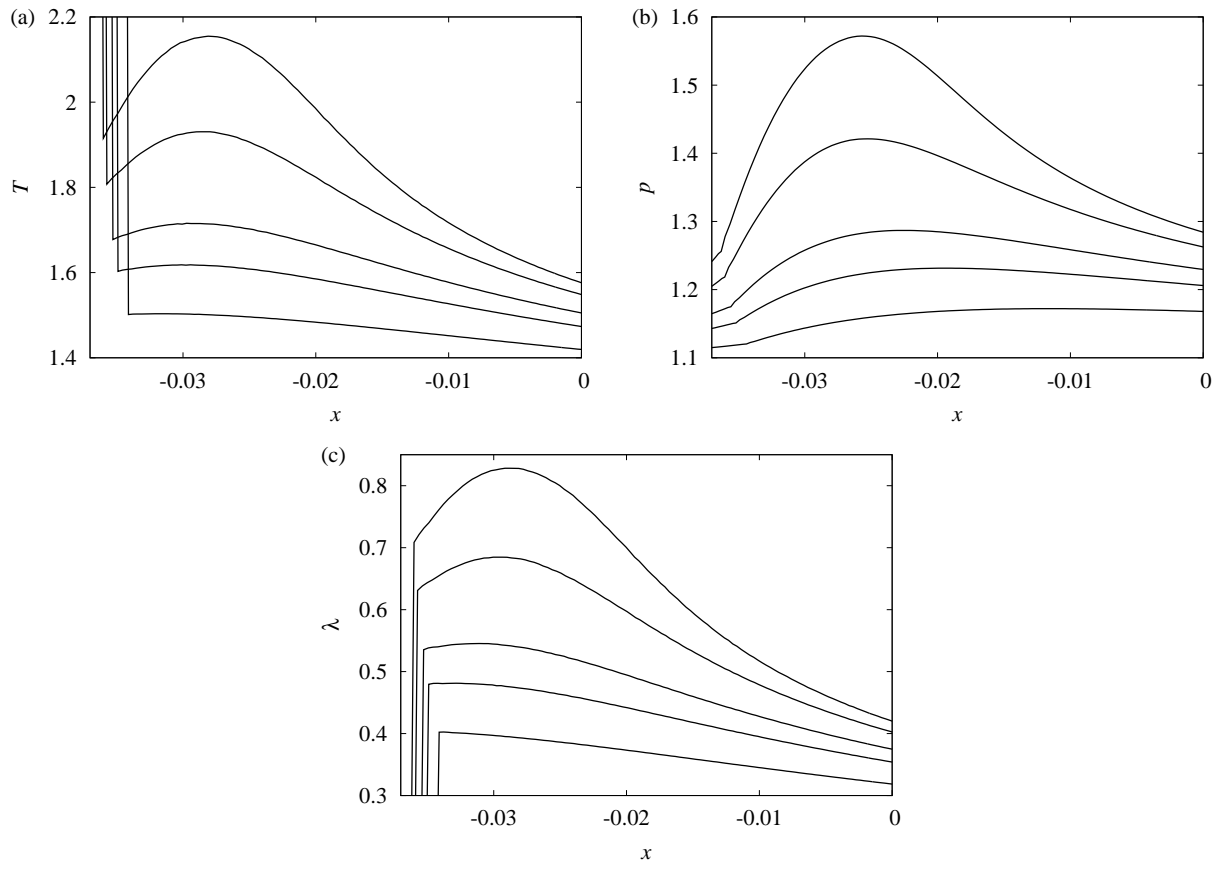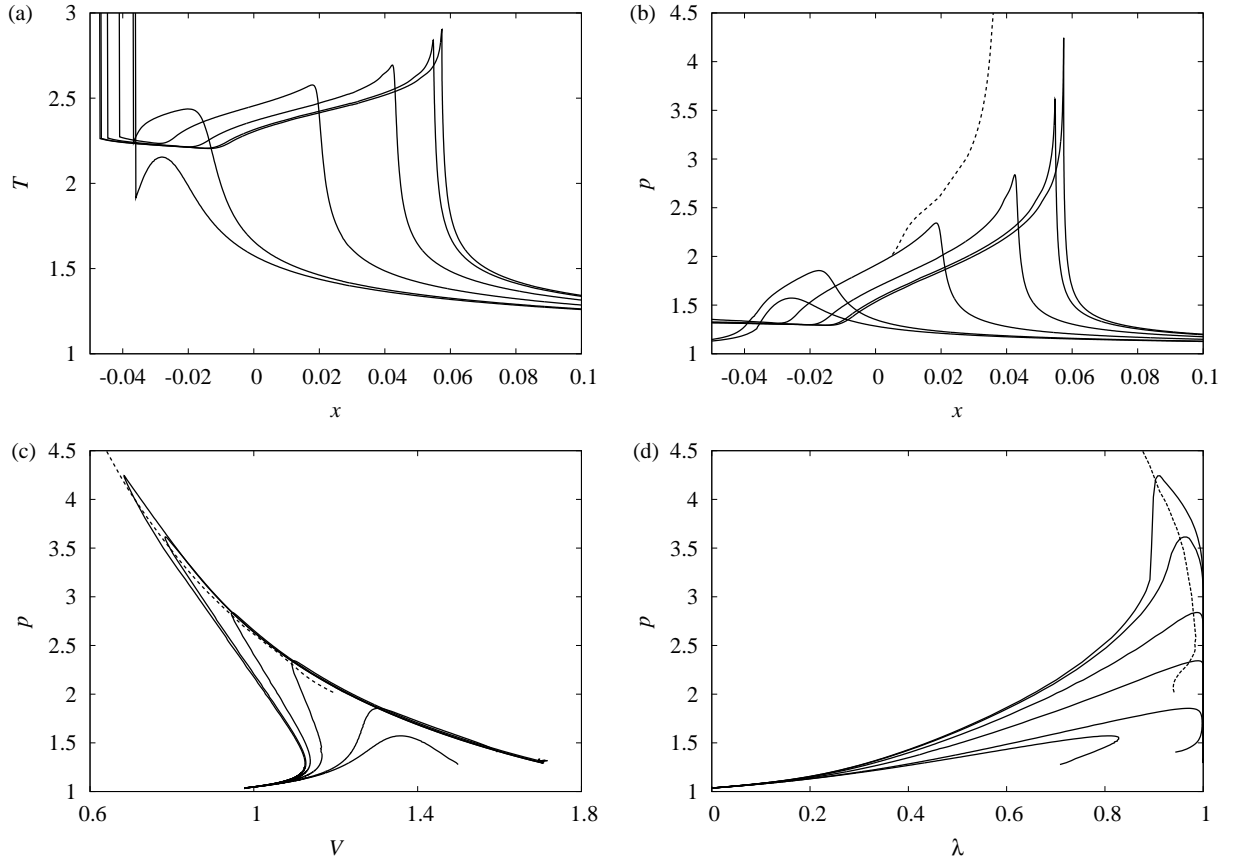
FIG. 7: Post-leading shock spatial profiles of (a) temperature and (b) pressure, and (c) pV and (d) $p\lambda$ diagrams of the region between the leading shock and contact surface, for $E = 15$ and $\alpha_0 = 0.5$, at times $t = 1.693$, 1.715, 1.737, 1.759, 1.770 and 1.776. Also shown as dotted lines are loci of the pressure maximum from the piston driven shock case ($\alpha_0 \to \infty$).
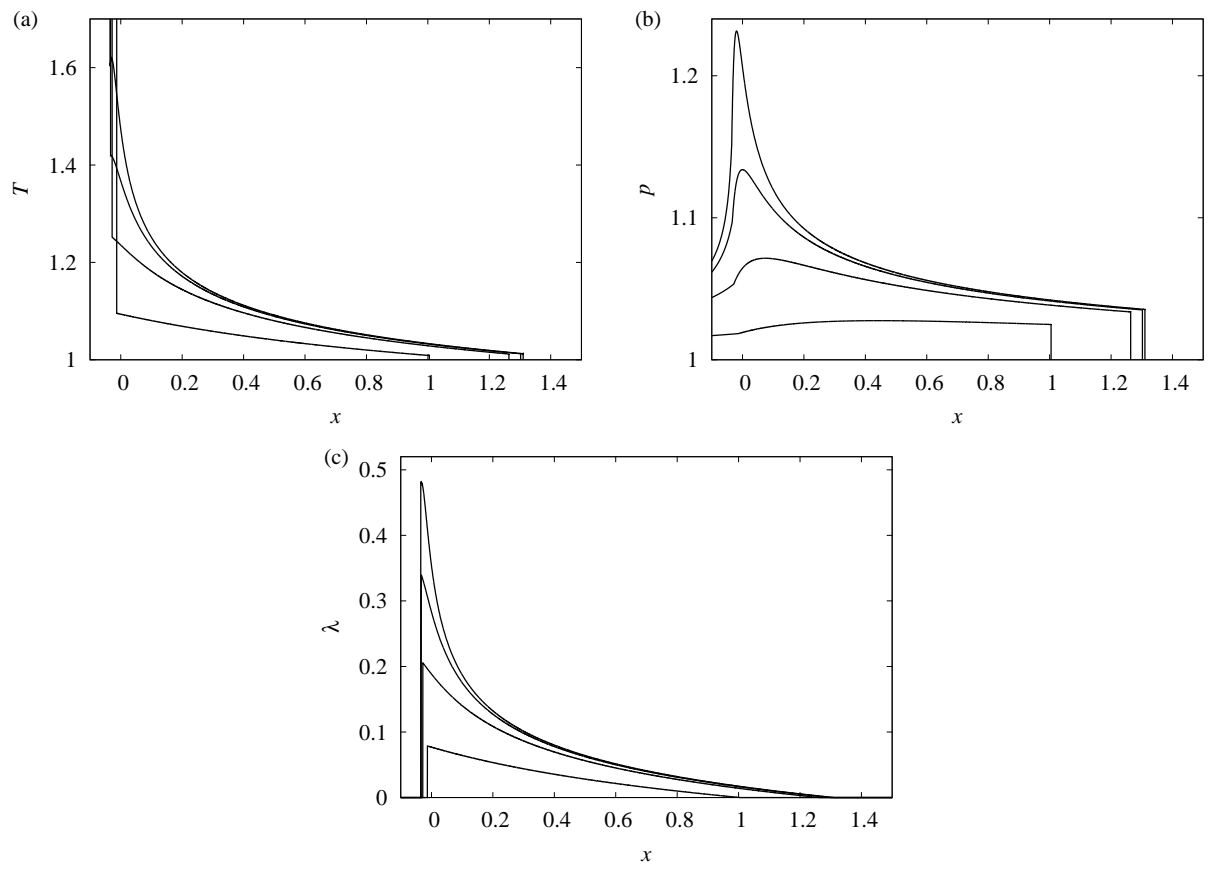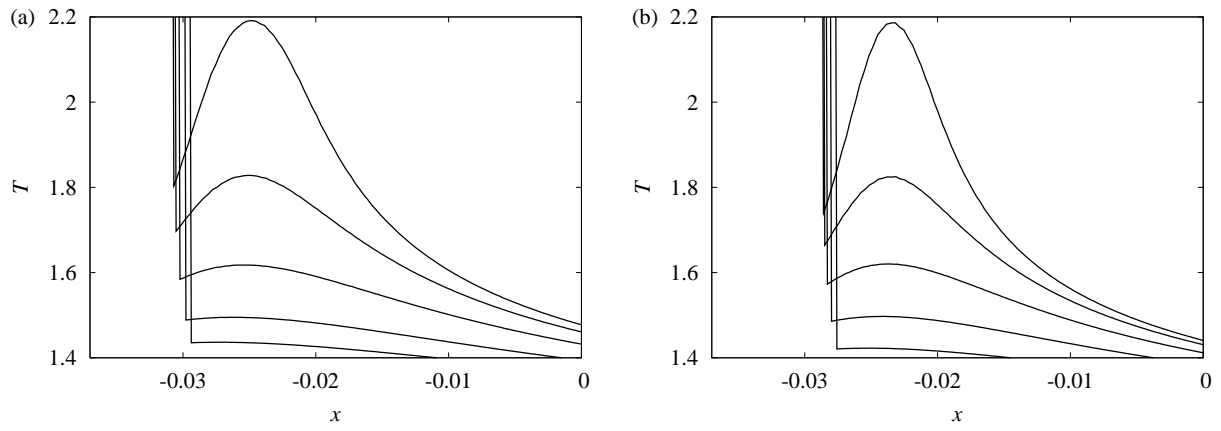
FIG. 8: Spatial profiles of (a) temperature, (b) pressure and (c) reaction progress variable, for $E = 20$ and $\alpha_0 = 0.5$, at times $t = 1.199$, 1.504, 1.549 and 1.558.

FIG. 9: Spatial profiles close to contact surface of (a) temperature, (b) pressure and (c) reaction progress variable, for $E = 20$ and $\alpha_0 = 0.5$, at times $t = 1.555$, 1.558, 1.560, 1.561 and 1.562.
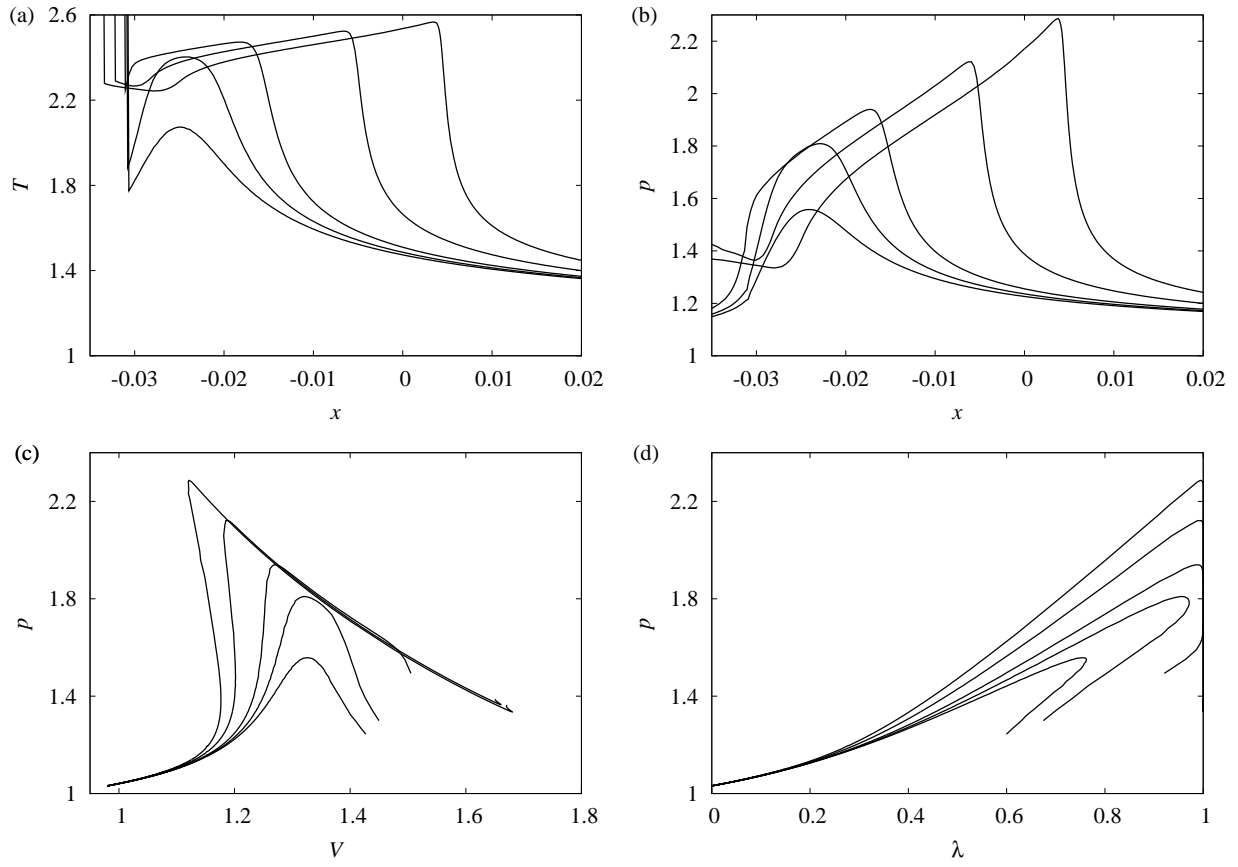
FIG. 10: Post-leading shock spatial profiles of (a) temperature and (b) pressure, and (c) pV and (d) $p\lambda$ diagrams of the region between the leading shock and contact surface, for $E = 20$ and $\alpha_0 = 0.5$, at times $t = 1.562$, 1.565, 1.572, 1.579, 1.583 and 1.584. Also shown as dotted lines are loci of the pressure maximum from the piston driven case ($\alpha_0 \to \infty$).

FIG. 11: Spatial temperature profiles close to contact surface for $\alpha_0 = 0.5$ and (a) $E = 22$ (shown at times $t = 1.5267$, 1.5290, 1.5311, 1.5322 and 1.5327) and (b) $E = 23$ (shown at times $t = 1.5159$, 1.5181, 1.5196, 1.5203 and 1.5207).

FIG. 12: Post-leading shock spatial profiles of (a) temperature and (b) pressure, and (c) pV and (d) $p\lambda$ diagrams of the region between the leading shock and contact surface, for $E = 22$ and $\alpha_0 = 0.5$, at times $t = 1.5326$, 1.5330, 1.5335, 1.5353 and 1.5376.
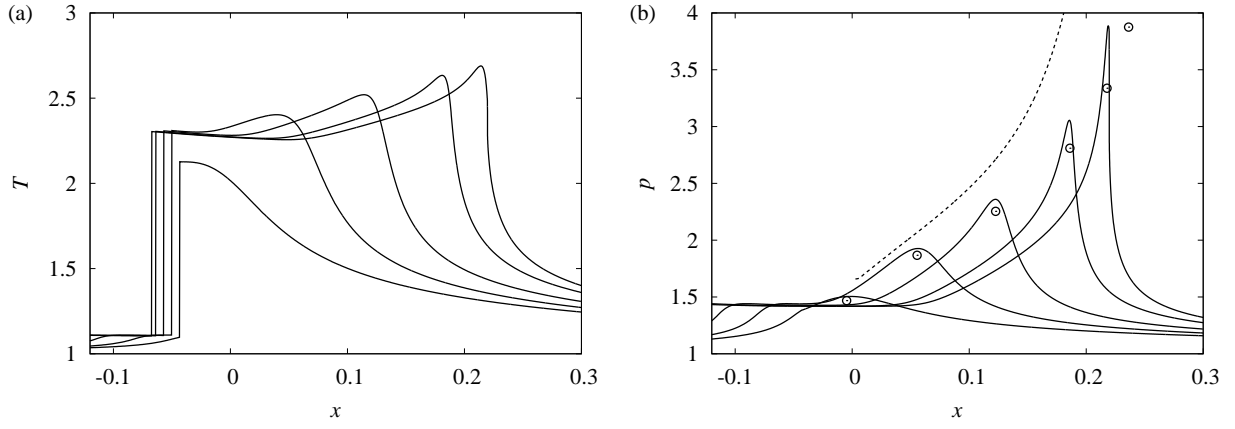
FIG. 13: Post-leading shock spatial profiles of (a) temperature and (b) pressure, for $E = 15$ and $\alpha_0 = 1$, at times $t = 1.640$, 1.662, 1.684, 1.706 and 1.718. Also shown as a dotted line is the locus of the pressure maximum from the piston driven case ($\alpha_0 \to \infty$), and as open circles the pressure maxima from the profiles shown in figure 7(b) for $\alpha_0 = 0.5$ (open circles).
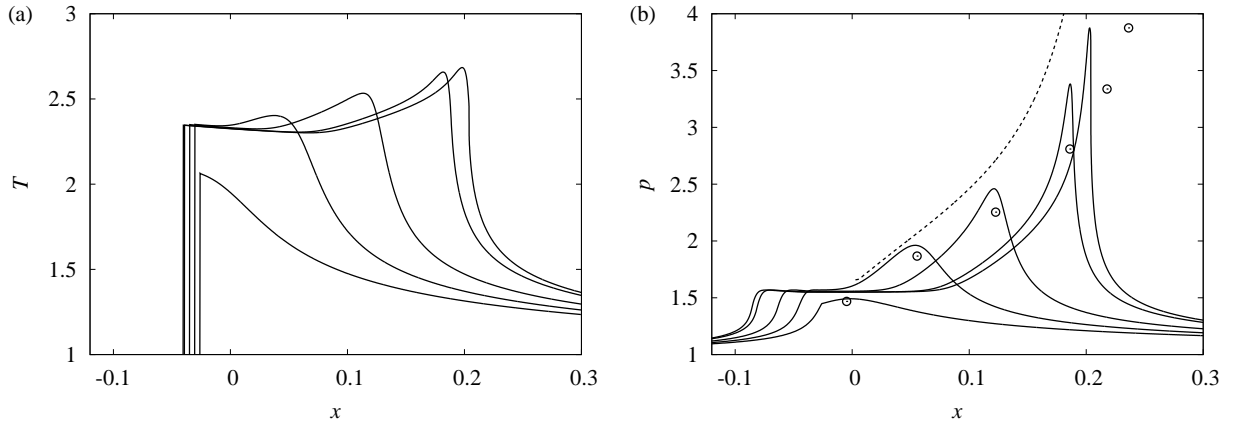

FIG. 14: Post-leading shock spatial profiles of (a) temperature and (b) pressure, for $E = 15$ and $\alpha_0 = 2$, at times $t = 1.588$, 1.612, 1.635, 1.657 and 1.663. Also shown as a dotted line is the locus of the pressure maximum from the piston driven case ($\alpha_0 \to \infty$), and as open circles the pressure maxima from the profiles shown in figure 7(b) for $\alpha_0 = 0.5$.
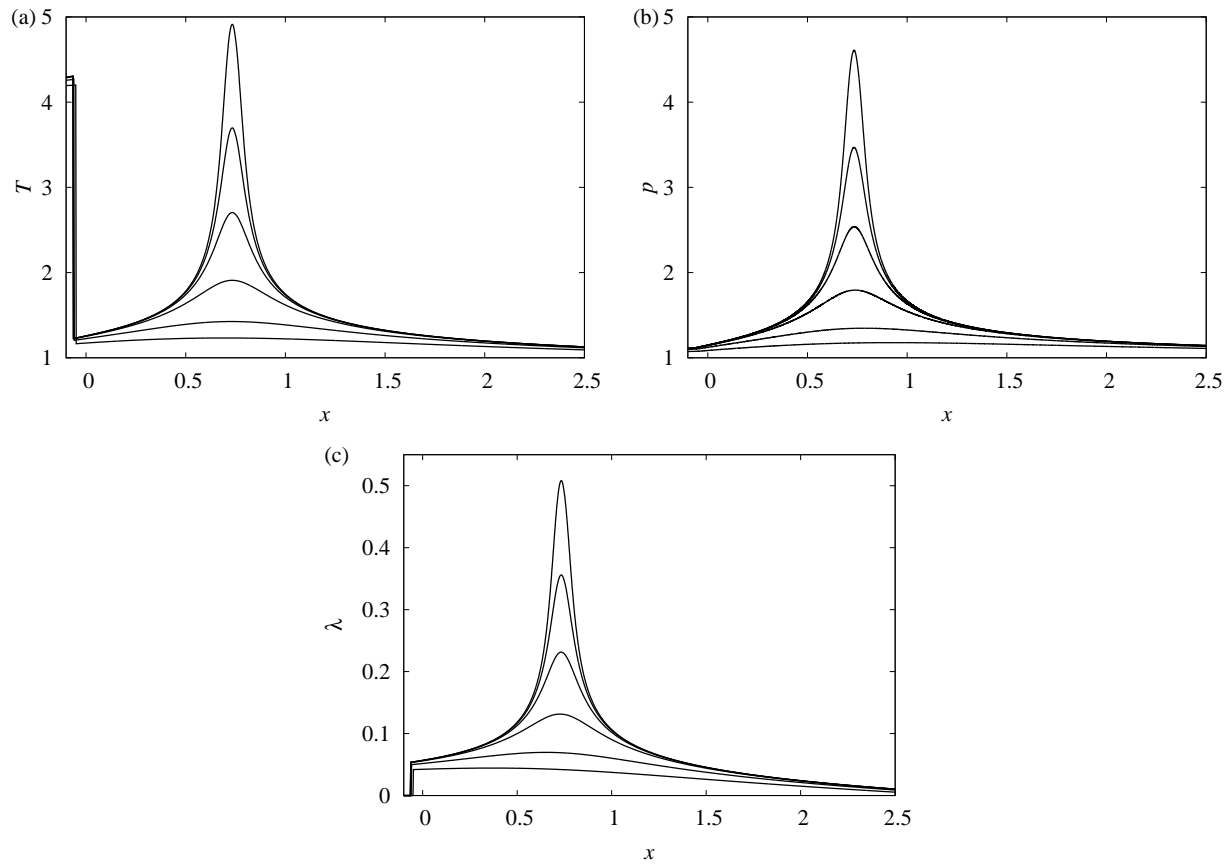
40

FIG. 15: Spatial profiles of (a) temperature, (b) pressure and (c) reaction progress variable, for $E = 15$, $\gamma = 3$, $\alpha_0 = 0.5$, at times $t = 2.1177$, 2.2092, 2.2383, 2.2423, 2.2430 and 2.2434.
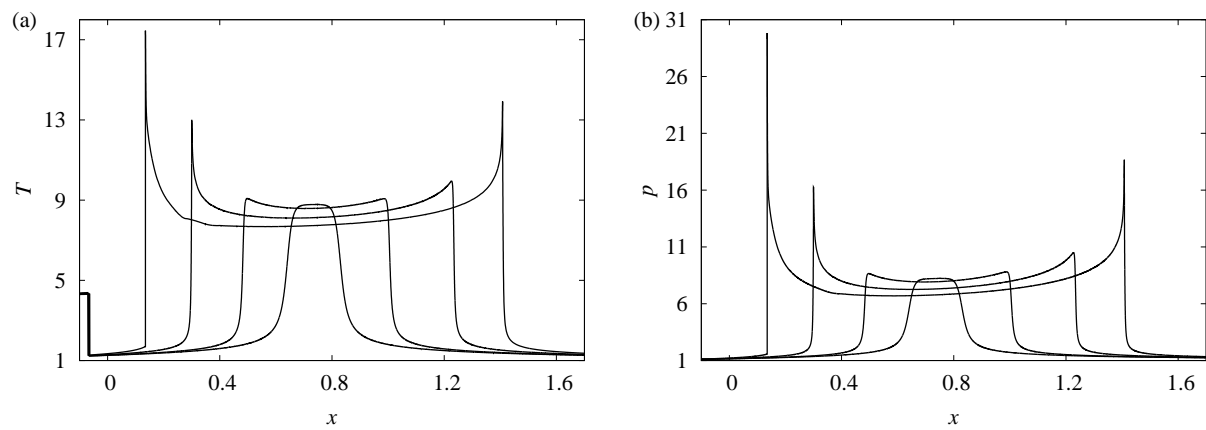

FIG. 16: Post-leading shock spatial profiles of (a) temperature and (b) pressure, for $E = 15$, $\gamma = 3$ and $\alpha_0 = 0.5$, at times $t = 2.245$, 2.252, 2.270 and 2.291.
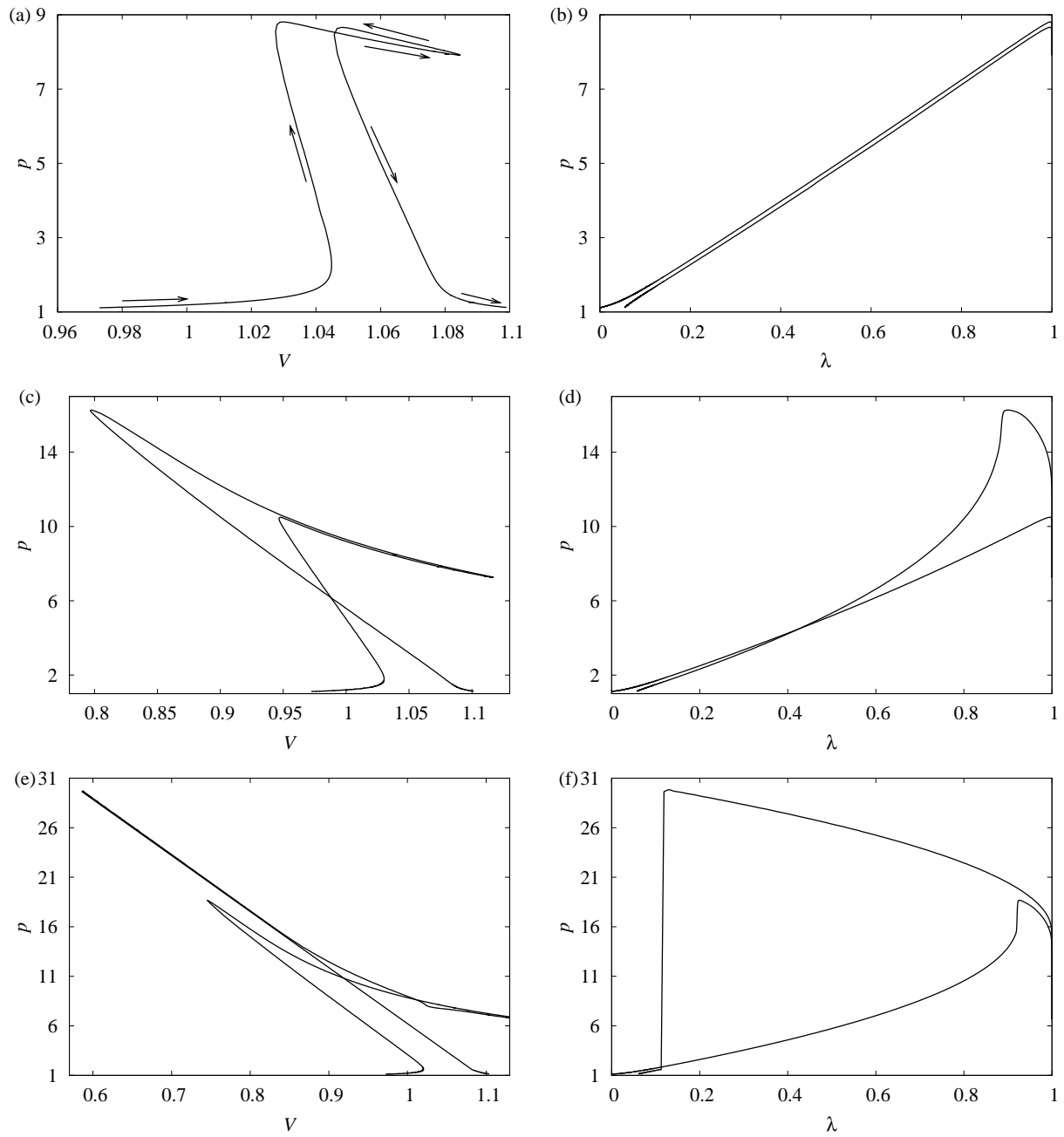
41

FIG. 17: pV and $p\lambda$ diagrams of the region between leading shock and contact surface, when $E = 15$, $\gamma = 3$ and $\alpha_0 = 0.5$, at times: (a), (b) $t = 2.252$; (c), (d) $t = 2.270$; (e), (f) $t = 2.291$. The arrows in (a) denote the direction of the trajectories corresponding to moving from the shock to the contact surface.

42